nature biomedical engineering

Article

https://doi.org/10.1038/s41551-023-01147-6

Small-molecule-mediated control of the anti-tumour activity and off-tumour toxicity of a supramolecular bispecific T cell engager

Received: 22 January 2023

Accepted: 24 October 2023

Published online: 20 February 2024

Check for updates

Ningqiang Gong[1], Xuexiang Han[1], Lulu Xue[1], Margaret M. Billingsley[1], Xisha Huang[1], Rakan El-Mayta[1], Jingya Qin[1], Neil C. Sheppard[2,3], Carl H. June[2,3] & Michael J. Mitchell[1,2,3,4,5,6,7,8,9]

The broader clinical use of bispecific T cell engagers for inducing anti-tumour toxicity is hindered by their on-target off-tumour toxicity and the associated neurotoxicity and cytokine-release syndrome. Here we show that the off-tumour toxicity of a supramolecular bispecific T cell engager binding to the T cell co-receptor CD3 and to the human epidermal growth factor receptor 2 on breast tumour cells can be halted by disengaging the T cells from the tumour cells via the infusion of the small-molecule drug amantadine, which disassembles the supramolecular aggregate. In mice bearing human epidermal growth factor receptor 2-expressing tumours and with a human immune system, high intravenous doses of such a 'switchable T cell nanoengager' elicited strong tumour-specific adaptive immune responses that prevented tumour relapse, while the infusion of amantadine restricted off-tumour toxicity, cytokine-release syndrome and neurotoxicity. Supramolecular chemistry may be further leveraged to control the anti-tumour activity and off-tumour toxicity of bispecific antibodies.

T cell therapies utilizing bispecific T cell engagers (BiTEs) have emerged as effective treatments for many types of blood cancers in the clinic[1–3], and they are currently being evaluated for solid tumour therapy[4,5]. BiTEs are antibodies that interact with both T cells and tumour cells[6] to induce tumour cell lysis via cell surface marker recognition[7,8]. For example, blinatumomab (Blincyto), the first BiTE therapy to receive the US Food and Drug Administration approval[9], links $CD3^+$ T cells to $CD19^+$ B cells, inducing T cell activation followed by serial T cell-mediated killing of malignant $CD19^+$ cells in acute lymphoblastic leukaemia[10,11], greatly improving patient outcomes[12,13]. There are several other BiTE therapies for glioma[14], lung cancer[15], B cell lymphoma[16], prostate cancer[17], pancreatic cancer[18] and breast cancer[19] under investigation in clinical trials. However, BiTE therapy can result in severe adverse effects such as on-target off-tumour toxicity, cytokine-release syndrome (CRS) and neurotoxicity[10,20], which can lead to patient death[21,22]. The on-target off-tumour toxicity arises in patients who have the target antigen expressed on both tumour and healthy tissue[23,24]. This expression pattern is typical for the vast majority of target antigens used in BiTE and chimeric antigen receptor (CAR) T cell therapies[23,25]. Human epidermal growth factor receptor 2 (HER2) is one example that

[1]Department of Bioengineering, University of Pennsylvania, Philadelphia, PA, USA. [2]Center for Cellular Immunotherapies, University of Pennsylvania, Philadelphia, PA, USA. [3]Department of Pathology and Laboratory Medicine, Perelman School of Medicine, University of Pennsylvania, Philadelphia, PA, USA. [4]Abramson Cancer Center, Perelman School of Medicine, University of Pennsylvania, Philadelphia, PA, USA. [5]Institute for Immunology, Perelman School of Medicine, University of Pennsylvania, Philadelphia, PA, USA. [6]Cardiovascular Institute, Perelman School of Medicine, University of Pennsylvania, Philadelphia, PA, USA. [7]Institute for Regenerative Medicine, Perelman School of Medicine, University of Pennsylvania, Philadelphia, PA, USA. [8]Institute for RNA Innovation, University of Pennsylvania, Philadelphia, PA, USA. [9]Center for Precision Engineering for Health, University of Pennsylvania, Philadelphia, PA, USA. e-mail: mjmitch@seas.upenn.edu

https://doi.org/10.1038/s41551-023-01147-6

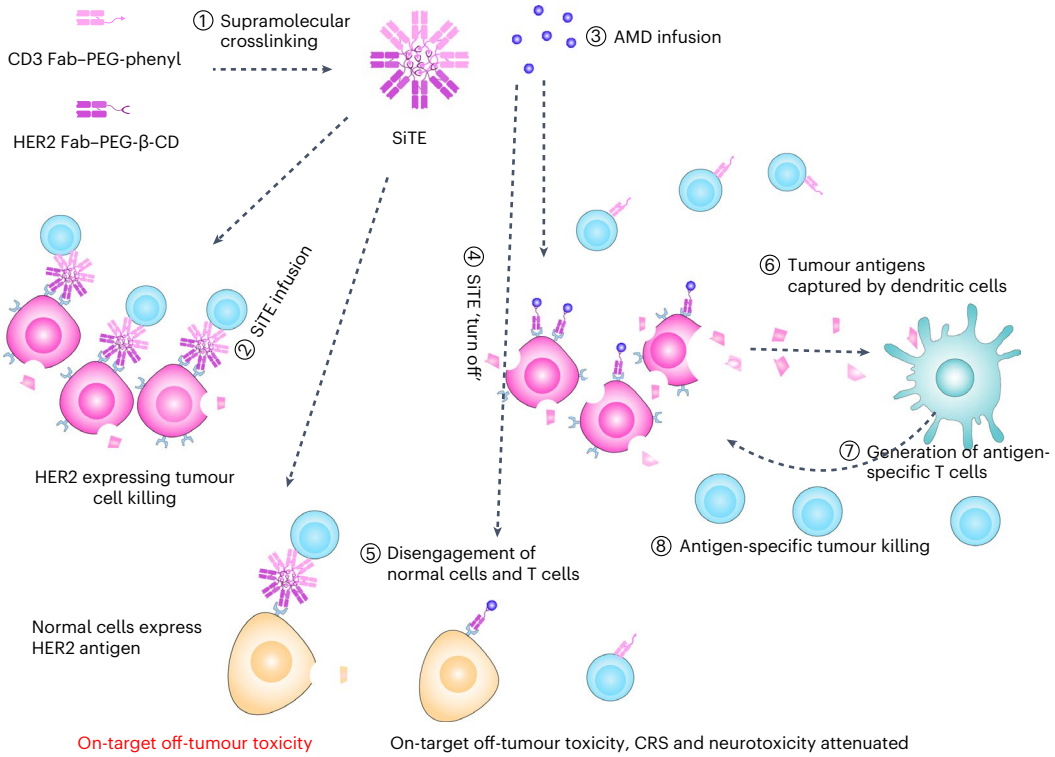

Fig. 1 | SiTE for cancer immunotherapy. The SiTE was prepared using a supramolecular chemistry-based method to assemble the Fab fragments of antibodies targeting both T cells and tumour cells (1). Once infused into a patient (2), SiTE can then engage both T cells and tumour cells to induce effective tumour cell killing. However, BiTE therapies, including SiTE, may also engage healthy tissue that expresses the target tumour antigen, resulting in on-target off-tumour toxicity. In addition, intensive tumour cell lysis and over-activation of innate immune cells such as monocytes and macrophages can also induce CRS and neurotoxicity. However, unlike traditional BiTEs, the SiTE can be disassembled using the small molecule AMD (3), halting off-tumour toxicity along with CRS and neurotoxicity upon detection (4 and 5). While infusion of AMD disengages T cells and tumour cells, which may induce tumour relapse, we found that high doses of SiTE greatly inhibited tumour cell growth and prevented tumour cell re-challenge, as this high dose induced effective in situ vaccination (6–8).

has some expression in healthy tissues as well as overexpression as high as 40- to 100-fold in tumours[26]. Such toxicity during HER2-based CAR T cell therapy was demonstrated when a patient with colorectal cancer received treatment that resulted in off-tumour targeting of their cardiopulmonary system, causing lethal toxicity[27]. In addition to on-target off-tumour toxicity, BiTE therapy-related CRS and neurotoxicity often occur in the clinic. BiTEs engage T cells and tumour cells very efficiently. However, intensive tumour cell lysis and over-activation of innate immune cells such as monocytes and macrophages leads to CRS and neurotoxicity[28]. The on-target off-tumour toxicity, CRS and neurotoxicity restrict the broader application of BiTEs. Thus, new strategies to help mitigate the toxicities associated with BiTEs are urgently needed in the clinic[29].

Studies have shown that supramolecular chemistry can be used to assemble proteins into one-, two- or three-dimensional structures[30], and their disassembly can be controlled using small molecules[31]. Inspired by this work, we present a switchable bispecific T cell nanoengager (SiTE) for controllable cancer immunotherapy (Fig. 1). Similar to traditional BiTEs, SiTE can engage T cells and tumour cells to efficiently induce tumour cell toxicity, but unlike traditional BiTEs, SiTE offers the ability to switch 'off' the therapy on demand. The on-target off-tumour toxicities, CRS and neurotoxicity caused by traditional BiTEs are difficult to control[32]. Here, we show that SiTE can be disassembled using an infusion of the small molecule amantadine (AMD)—allowing for these toxicities to be halted immediately upon infusion. AMD was first approved by the Food and Drug Administration in 1976 as an influenza A prophylactic and was subsequently approved to treat Parkinson disease[33]. As such, AMD represents an ideal candidate for regulating SiTE since its pharmacokinetic properties and safety have already been established. We evaluated the tumour cell lysing ability of these AMD-responsive SiTEs in both in vitro and in vivo models, and demonstrated the controllability of SiTE activity in vivo. Moreover, we developed a mouse model with stable human HER2 expression in healthy hepatic tissue and investigated the off-tumour toxicity caused by SiTE. In addition, we compared the therapeutic efficacy and anti-tumour activity of SiTE at a low and high dose. A humanized immune system mouse model was utilized to compare the anti-tumour efficacy, on-target off-tumour toxicity, CRS and neurotoxicity associated with SiTE and blinatumomab. In all, the results demonstrate that SiTE can induce anti-tumour activity without risking severe off-tumour toxicity, CRS and neurotoxicity, and may serve as a broadly applicable strategy for the design of future bispecific antibodies for cancer immunotherapy that avoids off-tumour toxicity.

Results and discussion

Synthesis and characterization of the SiTE

In this study, the SiTE was designed to bind both CD3 for T cell engagement and HER2 for tumour targeting[26], and disassemble when exposed to AMD (Fig. 2a). To begin SiTE synthesis, phenyl-modified poly(ethylene glycol) (PEG-phenyl) and β-cyclodextrin (β-CD)-modified PEG (PEG-β-CD) were synthesized[34] and then were characterized by using matrix-assisted laser desorption/ionization time of flight mass spectrometry (Supplementary Figs. 1 and 2). Fab fragments of antibodies for CD3 and HER2 were prepared using papain protease or IdeZ protease, respectively, and gel electrophoresis was used to confirm preparation of these Fab fragments (Supplementary Fig. 3a). The CD3 and HER2 Fab fragments were then treated with 2-iminothiolane to increase the number of thiol groups on their surface. The number

https://doi.org/10.1038/s41551-023-01147-6

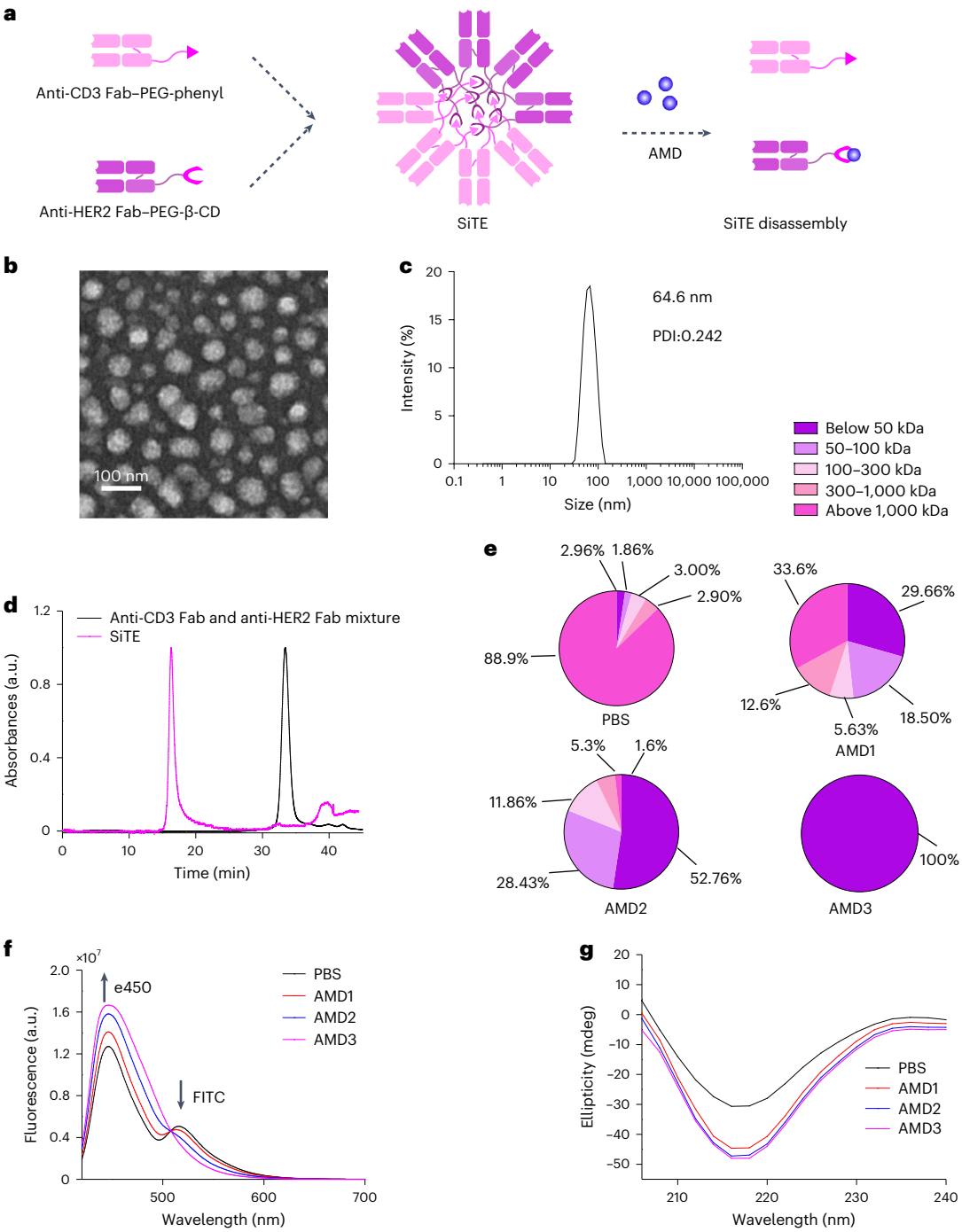

Fig. 2 | Synthesis and characterization of SiTE. a, Schematic of the synthesis of SiTEs. Phenyl-PEG–MAL conjugated to anti-CD3 Fab and β-CD-PEG–MAL conjugated to anti-HER2 Fab (random rather than site-specific conjugation was used for all experiments in this study) were mixed in PBS and self-assembled into SiTEs via supramolecular interactions between the phenyl group of anti-CD3 Fab–PEG-phenyl and the β-CD of anti-HER2 Fab–PEG-β-CD. The small molecule AMD, which has a high affinity for β-CD, can then be used to disturb the interactions between the phenyl group and β-CD to disassemble the SiTEs. **b**, A representative TEM image of SiTEs (scale bar, 100 nm). **c**, A representative DLS histogram of the SiTEs. PDI: polydispersity index. **d**, SEC of free CD3 Fab/HER2 Fab mixture and SiTEs. **e**, AMD-induced disassembly of SiTE was investigated using a two-step separation and quantification process, SiTE or SiTE mixed with increasing amounts of AMD (AMD1, 10 ng; AMD2, 500 ng and AMD3, 1,000 ng) confirming the dose-dependent disassembly of SiTE in the presence of AMD. **f**, Disassembly of SiTE by different amounts of AMD was also confirmed using a FRET experiment. SiTE assembled using e450-modified CD3 Fab and FITC-labelled HER2 Fab were mixed with different amounts of AMD and the emission spectra were measured. **g**, Circular dichroism spectra of SiTEs mixed with different amounts of AMD validated dose-dependent disassembly.

of thiol groups were increased to 4.7 and 4.9 for each CD3 and HER2 Fab, respectively (Methods)[35]. Then, CD3 and HER2 Fabs were conjugated to PEG-phenyl and PEG-β-CD, respectively (random rather than site-specific conjugation was used for all experiments in the current manuscript). These reactions to form CD3 Fab–PEG-phenyl and HER2 Fab–PEG-β-CD were performed at Fab to polymer (PEG conjugate) molar ratios of 1:1, 1:2, 1:3 and 1:4, and the products were characterized via gel electrophoresis (Supplementary Fig. 3b), revealing that the

conjugation of PEG-phenyl and PEG-β-CD to the Fab fragments did not induce aggregation at any of these ratios. Moreover, we also used size exclusion chromatography (SEC, Supplementary Fig. 4) to quantify the number of PEG-phenyl and PEG-β-CD conjugated to each CD3 and HER2 Fabs. The results indicated that approximately 1.12, 2.36, 3.40 and 4.84 MAL–PEG-phenyls were conjugated to each CD3 Fab when reacted at CD3 to PEG-phenyl ratios of 1:1, 1:2, 1:3 and 1:4, respectively. On average 1.15, 2.39, 4.09 and 4.91 MAL–PEG-β-CDs were conjugated to each HER2 Fab when reacted at HER2 Fab to MAL–PEG-β-CD ratios of 1:1, 1:2, 1:3 and 1:4, respectively.

We then assembled the SiTE by mixing CD3 Fab–PEG-phenyl with HER2 Fab–PEG-β-CD in phosphate buffered solution (PBS). Specifically, SiTE 1 was made using CD3 Fab–PEG-phenyl and HER2 Fab–PEG-β-CD that were both synthesized at the 1:1 Fab:PEG conjugate ratio while SiTE- 2, SiTE 3 and SiTE 4 used those made at 1:2, 1:3 and 1:4 Fab:PEG conjugate ratios, respectively. The phenyl groups from CD3 Fab–PEG-phenyl interact with the β-CD in HER2 Fab–PEG-β-CD mediated the assembly of the two antibodies. The interactions of phenyl groups in phenylalanine, tyrosine and tryptophan in CD3 antibody with β-CD in HER2 Fab–PEG-β-CD may have also contributed to the assembly of the SiTEs. Supplementary Fig. 5a,b shows transmission electron microscope (TEM) images and dynamic light scattering (DLS) size distribution data for SiTEs 1–4. The compositions of the four SiTEs were determined using a two-step separation and quantification method (Methods). The percentages of different components are shown in Supplementary Fig. 5c.

We then tested whether the addition of AMD[36–38]—which shows much higher affinity to β-CD compared with phenyl—can be used to separate the CD3 Fab–PEG-phenyl from the HER2 Fab–PEG-β-CD and ultimately 'switch off' the SiTEs. We mixed 10 μg of SiTEs with excess (500 μg) AMD and found that AMD induced complete disassembly of various SiTEs, demonstrating that AMD could be used to control SiTE structure and thus, potentially their activity (Supplementary Fig. 6a). Two additional small molecules—phenylalanine and tyrosine—were tested for their ability to separate these antibody fragments (Supplementary Fig. 6a). We found that both phenylalanine and tyrosine treatment induced the separation of the CD3 Fab from the HER2 Fab in SiTEs 1 and 2. However, neither phenylalanine nor tyrosine induced much separation in SiTEs 3 and 4 (Supplementary Fig. 6a). This is probably because SiTEs 1 and 2 consist mainly of the Fab dimer, which is formed via a single supramolecular interaction between the phenyl group and β-CD. However, SiTEs 3 and 4 contain mostly Fab nanoparticles that form via more stable multi-valent host–guest interactions between the phenyl group and β-CD. Next, to ensure the stability of SiTEs in the absence of AMD, SiTEs were stored at 4 °C in PBS, complete medium and mouse serum, and were then characterized for size over the course of 3 weeks. Over the course of this study, no changes in size were observed, suggesting that the SiTEs were mostly stable over this time period (Supplementary Fig. 6b–f). Finally, to compare their tumour killing efficacy, each SiTE was incubated with a mix of $HER2^+$ E0771 breast cancer cells and primary mouse T cells for 24 h (Supplementary Fig. 7a,b). The results showed HER2-specific engagement from the SiTEs and tumour cell toxicity, with SiTE 3 demonstrating the greatest tumour cell lysis (Supplementary Fig. 7b). Thus, SiTE 3 was selected for further exploration and is referred to as 'SiTE' throughout the rest of the study.

The SiTE was first characterized by using TEM imaging, DLS and SEC (Fig. 2b–d). Additionally, the affinity of the CD3 Fab and SiTE to CD3 antigen and the affinity of the HER2 Fab and SiTE to HER2 antigen were determined using a reported method[39,40]. As shown in Supplementary Fig. 8a,b, the dissociation constant (K_d) values of free CD3 Fab against CD3 protein and free HER2 Fab to HER2 protein were 1.08×10^{-9} M and 8.4×10^{-10} M, respectively. Surprisingly, the K_d value of the SiTE to CD3 antigen and HER2 antigen decreased to 1.33×10^{-10} M and 7.25×10^{-11} M, respectively. These results demonstrated that the conjugation and assembly of the CD3 and HER2 Fabs increased the avidity of both CD3 and HER2 Fabs. This may be a result of the multi-valent effect of the SiTE. We further investigated the binding of CD3 Fab, HER2 Fab and SiTE to their target antigens using quartz crystal microbalance (QCM, Supplementary Fig. 8c–g). SiTE showed improved binding to CD3 and HER2 protein-coated quartz crystals compared to free CD3 and HER2 Fabs (Supplementary Fig. 8c–g). These results further demonstrate the higher binding affinity of the SiTE to both CD3 and HER2 proteins. TEM and DLS confirmed a homogeneous SiTE solution with a diameter of approximately 66 nm. Further, SEC results (Fig. 2d) showed a main peak at around 16.3 min for SiTE, indicating an average composition of >20 Fab monomers per SiTE. We then used the two-step separation and quantification method to determine whether SiTE can be disassembled upon the addition of AMD (Fig. 2e). Our results showed that AMD can induce the disassembly of SiTE in a dose-dependent manner. To further confirm this AMD-induced SiTE disassembly, we also used fluorescence resonance energy transfer (FRET)[41]. Specifically, we modified the CD3 Fab with cell tracer 450 (e450) and modified the HER2 Fab with fluorescein isothiocyanate (FITC). Thus, minimal e450 signal and higher FITC signal is expected when CD3 and HER2 Fabs are bound, and higher e450 with no FITC signal would be indicative of dissociated Fabs. When characterizing the modified SiTE, strong FITC signal was observed in the absence of AMD, and increasing e450 was observed in the presence of increasing AMD doses, confirming dose-dependent AMD-induced disassembly (Fig. 2f). Finally, a circular dichroism experiment indicated that the secondary structure of the Fab was not affected (Fig. 2g). In all, these results confirmed the assembly and AMD-responsive disassembly of SiTE.

AMD-controllable activity of SiTEs in vitro

After synthesis and characterization of the AMD-responsive SiTE, we then tested the ability of SiTE to induce tumour cell T cell engagement and tumour cell lysis (Fig. 3a). We incubated E0771–HER2 cells with primary mouse T cells at a 1:1 ratio. Cells were then treated with SiTEs at varying concentrations for 4 h and observed under confocal laser scanning microscopy (Fig. 3b). In the untreated control group, cancer cells and T cells were randomly distributed, with few T cells and cancer cells engaged. However, in groups receiving 5 ng ml^{-1} of SiTE, ~10% of T cells were engaged with tumour cells, and this rate increased to ~90% when cells were treated with 20 ng ml^{-1} of SiTE. These results demonstrate that SiTE engaged tumour cells and T cells in a dose-dependent manner. To ensure the specificity of this engagement, we observed HER2-negative E0771 cells and T cells treated with SiTE and found negligible T cell–cancer cell engagement (Supplementary Fig. 7c). Further, treating the E0771–HER2 cells with free anti-CD3 Fab and anti-HER2 Fab before the addition of SiTE also did not result in T cell–cancer cell engagement

Fig. 3 | Small-molecule AMD controls SiTE activity in vitro. a, Schematic showing the mechanism of AMD-controllable SiTE. SiTE can effectively engage T cells and target cells to induce target cell lysis, but this engagement can be broken using the small molecule AMD. **b**, Confocal images of a mixture of E0771–HER2 cancer cells (red) and primary mouse T cells (blue). The cell mixtures were treated with different concentrations of SiTE (top) or with 20 ng ml^{-1} SiTE mixed with different amounts of AMD (bottom). **c**, E0771–HER2–Luc cells were mixed with mouse primary T cells and incubated with a mixture of anti-CD3 Fab and anti-HER2 Fab, different concentrations of SiTE or a mixture of SiTE and AMD for 24 h, and cancer cell viability was measured. **d**, IFN-γ levels in the culture medium in **c** were measured. **e**, E0771 or E0771–HER2 cells were mixed with mouse primary T cells and treated with 20 ng ml^{-1} SiTE in the presence of different concentrations of AMD for 24 h, and tumour cell viability was measured. **f**, Flow dot plots of the E0771–HER2 and T cell mixture after treatment with different formulations (left) and the subsequent quantification (right) ($n = 3$). The data in **c**, **d**, **e** and **f** are shown as the mean ± s.d. ($n = 3$–5) from independent experiments. Statistical differences were analysed by two-tailed unpaired Student's t-test.

https://doi.org/10.1038/s41551-023-01147-6

(Supplementary Fig. 7c), demonstrating that SiTE links T cells and cancer cells through the CD3 and HER2 surface antigens. Since the SiTE contains >20 Fabs, it is possible that it may induce T cell-to-T cell engagement and induce cytokine release. Upon investigation, we found that about 73.5% of T cells were in contact with tumour cells and about 18.7% of T cells were in contact with T cells (Supplementary Fig. 9a–c). The SiTE induced more cancer cell–T cell interactions than T cell–T cell interactions, potentially due to the lower K_d value of the SiTE to HER2

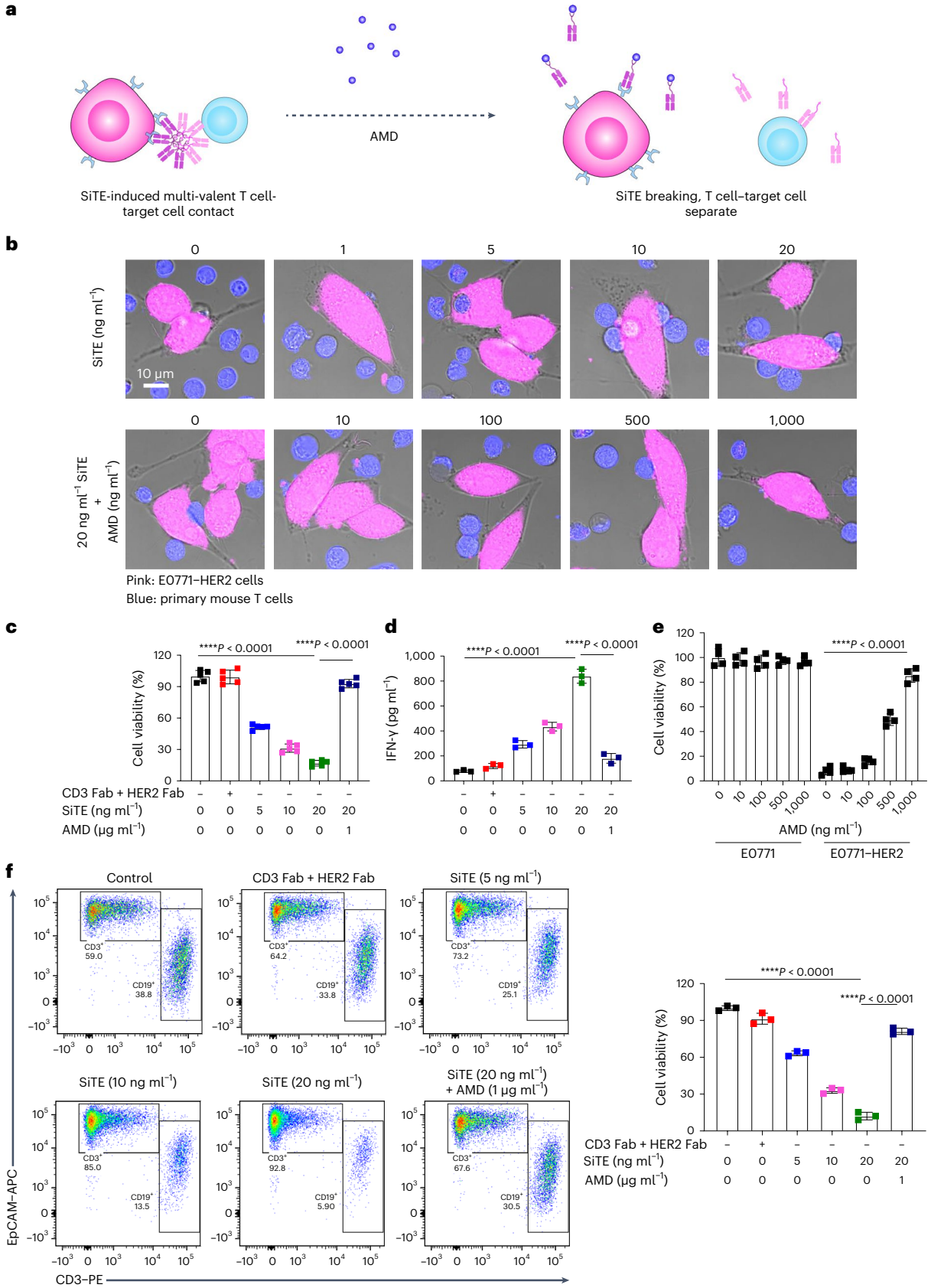

antigen (7.25×10^{-11} M) compared with the K_d of the SiTE to CD3 antigen (1.33×10^{-10} M) (Supplementary Fig. 8a,b). Moreover, we found a 20% increase in released T cell cytokines interleukin (IL)-2 and tumour necrosis factor (TNF)-α. These released cytokines may enhance the overall anti-tumour efficacy. To test whether SiTE could induce T cell crosslinking in vivo and their effect on toxic cytokine release, we injected SiTE to healthy mice. After 24 h, mouse blood was collected and the T cell crosslinking levels and IL-6 and TNF-α levels were measured. We found that SiTE induced about 2.5% of T cell crosslinking. However, the IL-6 and TNF-α concentration in the serum were comparable to those of a mixture of free CD3 and HER2 antibodies (Supplementary Fig. 9g–i), indicating low toxicity. SiTE treatment also did not lead to body weight loss or high fever (Supplementary Fig. 9j,k). Next, we tested whether AMD can disassemble SiTE and thus act to 'break' T cell–tumour cell engagement. T cells and E0771–HER2 tumour cells were mixed (1:1 ratio) and treated with 20 ng ml^{-1} SiTE for 4 h to induce T cell–tumour cell engagement. After the addition of varying concentrations of AMD, we found that AMD greatly reversed SiTE-induced engagement (Fig. 3b). A 100 ng ml^{-1} AMD treatment induced ~40% separation of conjugated cells while a 1 μg ml^{-1} AMD treatment resulted in nearly 100% separation, indicating an AMD dose-dependent disengagement. These results demonstrate that SiTE-induced T cell–cancer cell engagement can be quickly broken with the addition of AMD.

We then investigated whether the engagement of T cells and tumour cells by SiTE induces tumour cell lysis. E0771–HER2 cells and mouse primary T cells were mixed at a 1:1 ratio and treated with varying concentrations of SiTE (5–20 ng ml^{-1}), a 1:1 mixture of CD3 Fab and HER2 Fab, or a mixture of 20 ng ml^{-1} SiTE with 1 μg ml^{-1} AMD. After 24 h, E0771–HER2 cell viability was measured (Fig. 3c). The cells treated with a mixture of CD3 Fab and HER2 Fab did not show tumour cell lysis, and the cell viability was comparable to untreated controls. However, 5 ng ml^{-1} SiTE treatment induced ~50% E0771–HER2 cell death, and cell death increased to ~90% when cells were treated with 20 ng ml^{-1} SiTE. In contrast, the group treated with 20 ng ml^{-1} SiTE along with 1 μg ml^{-1} AMD had almost no tumour cell death compared with PBS, demonstrating that AMD can prevent SiTE-induced cancer cell lysis. In a similar experiment, SiTE treatment did not induce any toxicity to HER2-negative E0771 cells over a range of concentrations (Fig. 3e). Moreover, we found that pre-treating the cells with free CD3 Fab and HER2 Fab can prevent the tumour cell lysing ability of SiTE (Supplementary Fig. 7d). These results demonstrated that SiTEs induced antigen-specific cancer cell lysis. We also found that this specific cancer cell lysis induced by SiTE increases over time (Supplementary Fig. 10a). Enzyme-linked immunosorbent assays for interferon-γ (IFN-γ) and granzyme B further confirmed SiTE-induced cancer cell killing and AMD-responsive dysfunction of the SiTEs (Fig. 3c and Supplementary Fig. 10b–d). Together with the flow results (Fig. 3f), we demonstrate that the SiTE-induced cancer cell killing can be controlled in vitro using AMD.

Finally, to observe whether the SiTE could be applied to target other cancers, we designed SiTE using anti-human CD3 Fab and anti-human CD19 Fab and tested its ability to induce T cell–cancer cell engagement, cancer cell lysis and AMD responsiveness (Supplementary Fig. 11). We found comparable T cell–cancer cell engagement, tumour cell lysis and AMD-dependent disassembly in the CD19-targeted SiTE, indicating the versatility and broad potential for this SiTE strategy. In all, these results demonstrate the efficacy of SiTE for tumour cell lysis in vitro and validate the ability of AMD to stop SiTE activity.

AMD-controllable activity of SiTEs in vivo

Encouraged by the results from the in vitro experiments, we next evaluated the controllable activity of SiTE in vivo. To first assess safety for in vivo experiments, SiTE were incubated with red blood cells and were found to cause negligible red blood cell lysis at concentrations as high as 2 mg ml^{-1} (Supplementary Fig. 12). As several studies have demonstrated that PEGylation can greatly improve the blood circulation of many protein-based drugs[42,43], we next investigated whether the supramolecular linker in SiTE increased blood circulation time (Supplementary Fig. 13). The results demonstrated that SiTE has a half-life of around 24 h, and that ~25% of SiTE remained in blood 48 h post-infusion. As compared with blinatumomab, a traditional BiTE with a short half-life of 2.11 h (ref. 44), SiTE exhibited an enhanced blood circulation time, which is important for anti-tumour applications. In the clinic, blinatumomab may naturally possess a switch off mechanism since it can be quickly cleared from the blood due to its short half-life. However, we found that even though blinatumomab can be quickly cleared after intravenous (i.v.) injection (Supplementary Fig. 14a,b), it accumulated greatly in the spleens of healthy mice with a humanized immune system (Supplementary Fig. 14c). Moreover, high accumulation of blinatumomab in the tumours, livers and spleens (Supplementary Fig. 14c) was also observed in Raji tumour-bearing humanized mice that express human CD19 antigen in the liver. We also analysed the biodistribution of our SiTE both in healthy NOD scid gamma (NSG) mice and in Raji tumour-bearing humanized NSG mice that express CD19 antigen in the liver. Our SiTE possessed a similar biodistribution pattern to blinatumomab in both groups of mice (Supplementary Fig. 14d). The potential toxicity induced by such high accumulation of both blinatumomab and our SiTE makes a switch off mechanism necessary to mitigate toxicity.

We then examined whether SiTE can target tumour tissues in vivo. We first constructed an E0771–HER2 tumour model before injecting the mice i.v. with Cy7-labelled SiTE (Cy7 labelled on CD3 Fab), a Cy7-labelled Fab nanoparticle made up of 50% HER2 Fab isotype and 50% CD3 Fab (Cy7 labelled on CD3 Fab), or a Cy7-labelled Fab nanoparticle made up of 50% CD3 Fab isotype and 50% HER2 Fab (Cy7 labelled on the CD3 Fab isotype) at 0 h. After 24 h, the mice were euthanized and the Cy7 signal in different organs and tumour was measured (Supplementary Fig. 15). The results showed that the SiTE mainly accumulated in the tumour and spleen. However, the nanoparticle with a HER2 Fab isotype mainly accumulated in the spleen. This is because CD3 Fab in this nanoparticle can target T cells in the spleen, while the HER2 Fab isotype cannot recognize HER2 (Supplementary Fig. 15b). The nanoparticle with a CD3 Fab isotype, however, mainly accumulated in the tumour tissue. These results demonstrate that the presence of HER2 Fab in SiTE can help to target tumour tissue (Supplementary Fig. 15c). Moreover, we confirmed that SiTE can effectively penetrate and accumulate deep in tumour spheroids (Supplementary Fig. 15d–f).

We sought to evaluate whether AMD can be used to break down the SiTE in vivo. We modified Cy7 to the CD3 Fab and assembled the Fab with HER2 Fab to formulate SiTE–Cy7. SiTE–Cy7 was i.v. injected to E0771–HER2 tumour-bearing mice at 0 h. At 18 h post-SiTE–Cy7 injection, AMD dispersed in PBS or AMD dispersed in 5% polyoxyethylene castor oil was i.v. injected into mice. Mice were euthanized 6 h later and the Cy7 signal in different organs and tumour was measured using an in vivo imaging system (IVIS). As shown in Extended Data Fig. 1, the SiTE-only group showed fluorescence signal in both the tumour and spleen. However, we found that AMD dispersed in PBS did not induce a complete breakdown of the SiTE, with about a 46% decrease in Cy7 signal in the tumour (Extended Data Fig. 1a,b). This may be attributed to insufficient tumour accumulation due to the short half-life of AMD (Extended Data Fig. 1d). However, we found that dispersing AMD in 5% polyoxyethylene castor oil can help to enhance the half-life of AMD to about 24 h and this can induce an over 78% Cy7 signal decrease compared with PBS treatment (Extended Data Fig. 1e). This is likely due to SiTE disassembly in the presence of AMD, allowing the Cy7–CD3 Fab to separate from the tumour-targeting HER2 Fab. A kinetic study showed that AMD first reached the liver and then distributed to major organs and tumour tissues (Extended Data Fig. 1f,g). Moreover, a higher Cy7 signal was detected in the kidney (Extended Data Fig. 1c), indicating that the disassembled free Fab undergoes clearance in the kidney

https://doi.org/10.1038/s41551-023-01147-6

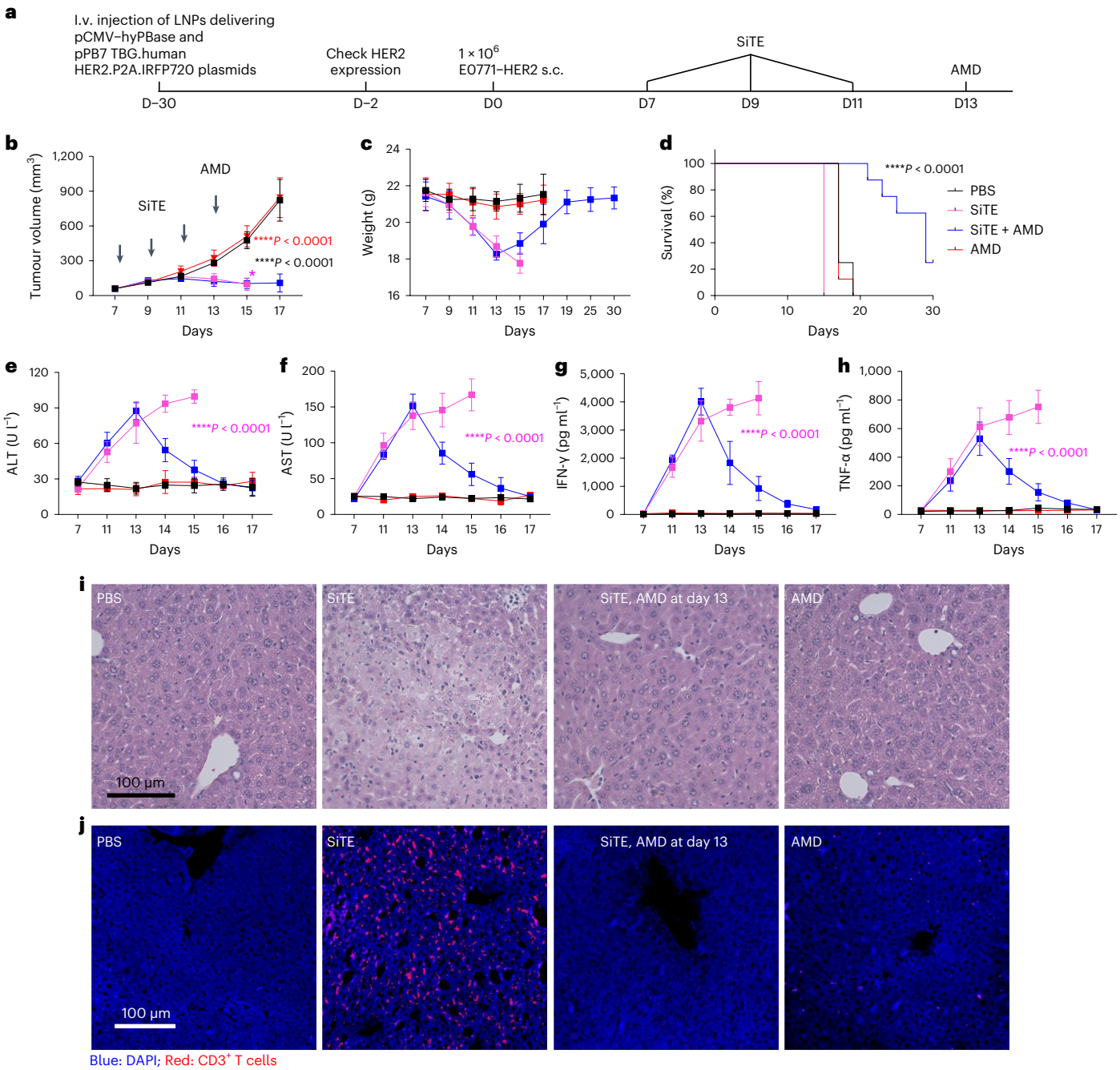

Fig. 4 | AMD reduces the on-target off-tumour toxicity of SiTE in vivo. **a**, A mouse model with expression of human HER2 antigen in the liver was constructed using a piggyback transposon system delivered via LNPs encapsulating two plasmids, pCMV–hyPBase and pPB7 TBG.human HER2.P2A.IRFP720, at day −30 (D−30). One million (10^6) E0771–HER2 tumour cells were injected subcutaneously (s.c.) into the right flank at day 0. After tumour size reached 50 mm^3 (day 7), PBS, SiTE or AMD were i.v. injected three times every 2 days. When an approximate 15% decrease in body weight, indicative of toxicity, was observed on day 13, half of the mice that had received SiTE were given an i.v. injection of AMD. **b**–**d**, Mouse tumour growth curves (**b**), measurements of mouse body weight (**c**) and survival curves (**d**), $n = 8$ mice. The P value in **d** was determined using a log-rank (Mantel–Cox) test. The red stars in **b** and **c** indicate that mice were euthanized. **e**–**k**, Measurements of markers for inflammation and toxicity including ALT (**e**), AST (**f**), IFN-γ (**g**) and TNF-α (**h**) levels in mouse blood at different timepoints, $n = 3$ mice. **i**, All mice were euthanized by day 19, and mouse livers were collected. Haematoxylin and eosin staining was conducted to detect liver damage in different groups. Scale bar, 100 μm. **j**, Immunofluorescence imaging of $CD3^+$ T cells in liver tissue. The data in **b** and **e**–**h** are shown as the mean ± s.d. ($n = 5$). P values are indicated. Blue, SiTE versus SiTE + AMD at day 15; pink, blinatumomab versus SiTE + AMD at day 15, ****$P < 0.0001$, analysed by two-tailed unpaired Student's t-tests.

(Extended Data Fig. 1h,i). AMD was also detected to be cleared from the urine (Extended Data Fig. 1j), which is consistent with a clinical report[45]. These results demonstrate that the SiTE can accumulate in tumour tissue, and an infusion of the small molecule AMD can disassemble SiTE to release the CD3 Fab from the tumour tissue. Most supramolecular chemistry-based strategies for controllable chemotherapeutic release have only been tested in in vitro studies[36,46,47], and only a few in vivo controllable drug release strategies have been reported[48,49]. These previous investigations may have been limited to mostly in vitro studies because the developed technologies require internalization by cancer cells, and

it is difficult to precisely deliver multiple cargoes into the same cancer cells in vivo[36,46,47]. However, in this study, the SiTE links T cells and cancer cells while retained on the cell surfaces, which allows AMD to bind and control the separation of anti-CD3 Fab from anti-HER2 Fab. This advantage makes the supramolecular chemistry-based controllable SiTE system uniquely useful in vivo.

With confirmed tumour accumulation, we then investigated whether the target cell lysing capacity of SiTE can be controlled via AMD administration in vivo. We constructed an E0771–HER2 tumour model, and mice were treated with three i.v. injections of PBS, SiTE (1 mg kg^{-1}), SiTE pre-mixed with 100 μg AMD, SiTE pre-mixed with 5 μg AMD, SiTE followed by one infusion of 100 μg AMD at day 13, or AMD (Extended Data Fig. 2a). Tumour size and mouse weight were monitored. As shown in Extended Data Fig. 2b–d, SiTE in the absence of AMD greatly inhibited tumour growth, as the tumour sizes in mice receiving SiTE reached ~70 mm^3 at day 23 whereas untreated tumour sizes were ~650 mm^3, supporting that SiTE induces efficient target cell lysing (Extended Data Fig. 2c,d). However, in mice treated with SiTE pre-mixed with AMD, the target cell lysing ability was attenuated, as tumour size was ~100 mm^3 in mice treated with SiTE pre-mixed with 5 μg AMD, and ~600 mm^3 in mice treated with SiTE pre-mixed with 100 μg AMD. These results suggest that pre-incubation of AMD with SiTE disassembled the SiTE and thus reduced tumour inhibition. In mice receiving the SiTE followed by 100 μg AMD at day 13, tumour growth was greatly inhibited until AMD infusion. However, after the AMD infusion (day 13), tumour growth continued, resulting in final tumour sizes of ~650 mm^3 at day 29 (Extended Data Fig. 2d). These results demonstrate that the target cell lysing capacity of SiTE can be controlled using AMD.

Minimal changes in mouse weight were observed across the different groups (Extended Data Fig. 2e), probably because the HER2 antigen is not expressed on normal mouse cells, preventing toxicity from on-target off-tumour activity. At day 23, all mice were euthanized, and tumour tissue was collected to determine total lymphocyte and $CD3^+$ T cell infiltration using flow cytometry and immunofluorescence imaging. We found that both $CD45^+$ lymphocytes and $CD3^+$ T cells were greatly increased in the tumour tissue of mice treated with SiTE compared with PBS-treated mice (Extended Data Fig. 2f,g and Supplementary Fig. 16). However, groups receiving SiTE pre-mixed with AMD displayed lower rates of immune cell infiltration into tumour tissue, and the group receiving an infusion of AMD after SiTE treatment saw minimal infiltration as well, demonstrating that AMD infusion probably reversed any infiltration induced by the SiTE. Further, histology experiments showed that the SiTE induced substantial tumour cell death in E0771–HER2 tumour tissue (Supplementary Fig. 17) and AMD can greatly control the activity of SiTE in vivo.

After observing the ability of SiTE to induce tumour infiltration and the potential of AMD to reverse it, a separate animal experiment was performed to assess T cell infiltration in tumour tissue at different timepoints, including before and after an AMD infusion (Extended Data Fig. 3). The results showed that SiTE greatly improved T cell infiltration, but following AMD infusion, the number of T cells in the tumour tissue greatly decreased (Extended Data Fig. 3), further confirming the controllable activity of SiTE. Additionally, to confirm that this impact on the tumour tissue was HER2 specific, we evaluated SiTE activity in a HER2-negative E0771 tumour model (Supplementary Fig. 18). We found that SiTE did not inhibit tumour growth, and T cell infiltration in HER2-negative E0771 tumour tissue also was not affected when mice were treated with SiTE and/or AMD. These results show that tumour cell–T cell engagement and tumour cell lysis induced by SiTE is HER2 antigen specific. Altogether, our results demonstrate that SiTE can substantially and specifically inhibit tumour growth in vivo and that this can be reversed using AMD.

AMD alleviates the on-target off-tumour toxicity of SiTE in vivo

The June group recently reported a mouse model with stable human HER2 antigen expression in the mouse liver[50]. They used a hydrodynamic injection[51] method to deliver a transposase plasmid and transposon plasmid encoding human HER2 antigen and a near-infrared fluorescent protein (IRFP) reporter to the mouse liver. Using this method, they found that the HER2 antigen was then stably expressed on mouse liver cells[50]. Here, we modified the construction of this mouse model and delivered the two plasmids using a lipid nanoparticle (LNP)[52,53] (Supplementary Fig. 19). Notably, we found higher IRFP and HER2 expression in mice treated with LNPs at a lower dose of plasmids compared with those treated with plasmids via the hydrodynamic injection method (Supplementary Fig. 19). We then constructed an E0771–HER2 tumour model in mice with HER2 expression in the liver (Fig. 4a). After the tumour size reached 100 mm^3, mice were i.v. injected with PBS, SiTE or free AMD. Half of the group receiving SiTE on days 7, 9 and 11 also received AMD on day 13. The mice were then monitored for tumour growth, body weight and survival (Fig. 4b–d). The results showed that SiTE greatly suppressed tumour growth, but they also induced substantial weight loss. This is probably due to off-tumour toxicity caused by the HER2 antigen expression in mouse liver cells resulting in liver cell lysis. Interestingly, on day 13, when half of the SiTE treated mice received 100 μg AMD to disassemble SiTE, the group of mice receiving AMD had gradual increases in body weight and recovered to a normal range, while those without an AMD infusion had to be euthanized due to continued weight loss. In the SiTE + AMD group (Fig. 4d), the tumours grew bigger and the mice were euthanized when the tumour size reached 700 mm^3.

To better characterize the weight loss seen in the SiTE-only treatment group, we conducted a separate animal experiment to analyse the alanine aminotransferase (ALT), aspartate aminotransferase

Fig. 5 | High doses of SiTE induce a strong tumour-specific T cell immune response. a, We constructed the mouse model of HER2 expression in the liver, and constructed the E0771–HER2 tumour model. Seven days later, mice were treated with an i.v. injection of PBS, a low dose of SiTE (1 mg kg^{-1}), a high dose of SiTE (5 mg kg^{-1}) or AMD on day 7 (D7), day 9 (D9) and day 11 (D11). At day 13, AMD was given to the groups receiving SiTE. Some mice were given the AMD before day 13 upon the observation of >15% body weight loss. **b**, Tumour growth curves are shown as an average of the eight mice in each treatment group for days 0–17 and each mouse is graphed separately for days 0–60. To assess the mechanism by which the high-dose SiTE group showed an improved anti-tumour effect, we performed an additional animal experiment using the same model and treatment groups, with tumour isolation on day 17. CR: complete remission. Q1: $FoxP3^+CD25^-$, Q2: $FoxP3^+CD25^+$, Q3: $FoxP3^-CD25^+$, Q4: $FoxP3^-CD25^-$. **c**–**f**, Immune cell infiltration in tumour tissue was analysed using flow cytometry. $CD25^+FoxP3^+$ Treg numbers and PD1 expression on T cell surface in each group. **g**,**h**, The central memory ($CD44^+CD62L^+$) and effector memory ($CD44^+CD62L^-$) cell populations in the mouse spleen. To investigate whether an immune memory effect was induced, E0771–HER2 tumour-bearing mice were treated with high doses of SiTE and the tumour-free mice in this group were then rechallenged with E0771–HER2 or E0771 cells. Mice pre-treated with either PBS or AMD and challenged with E0771–HER2 were used as controls. Group R1: healthy mice were treated with PBS at days −43, −41 and −39. The mice were challenged with E0771–HER2 cells at day 0. Group R2: E0771–HER2 tumour-bearing mice were treated with a high dose of SiTE at days −43, −41 and −39, AMD was i.v. injected at day −37. The tumour-free mice were rechallenged with E0771–HER2 cells at day 0. Group R3: E0771–HER2 tumour-bearing mice were pre-treated with high dose of SiTE at days −43, −41 and −39. AMD was i.v. injected at day −37. The mice were rechallenged with E0771–HER2 cells at day 0. Group R4: healthy mice were treated with AMD at day −37 and the mice were challenged with E0771–HER2 cells at day 0. **i**,**j**, $CD8^+$ T cell infiltration in the rechallenged tumour tissue was detected by immunofluorescence. **k**,**l**, $CD4^+$ T cell infiltration in the tumour tissue detected by immunofluorescence. The data in **d**, **f**, **h**, **j** and **i** are shown as the mean ± s.d. ($n = 3$) from three independent experiments. *P* values indicated in the figures were analysed by two-tailed unpaired Student's *t*-tests.

https://doi.org/10.1038/s41551-023-01147-6

(AST), IFN-γ and TNF-α levels in the mouse blood (Fig. 4e–h). The results showed that SiTE treatment increased ALT and AST levels in the blood, indicating severe liver cell damage. Moreover, IFN-γ and TNF-α levels in blood also increased in mice treated with SiTE (Fig. 4g,h), suggesting that SiTE induced T cell engagement and target cell lysis. However, ALT and AST returned to lower levels 24 h after AMD infusion, demonstrating that AMD can stop the liver cell damage caused by SiTE and that the response is rapid (Fig. 4e,f). We also

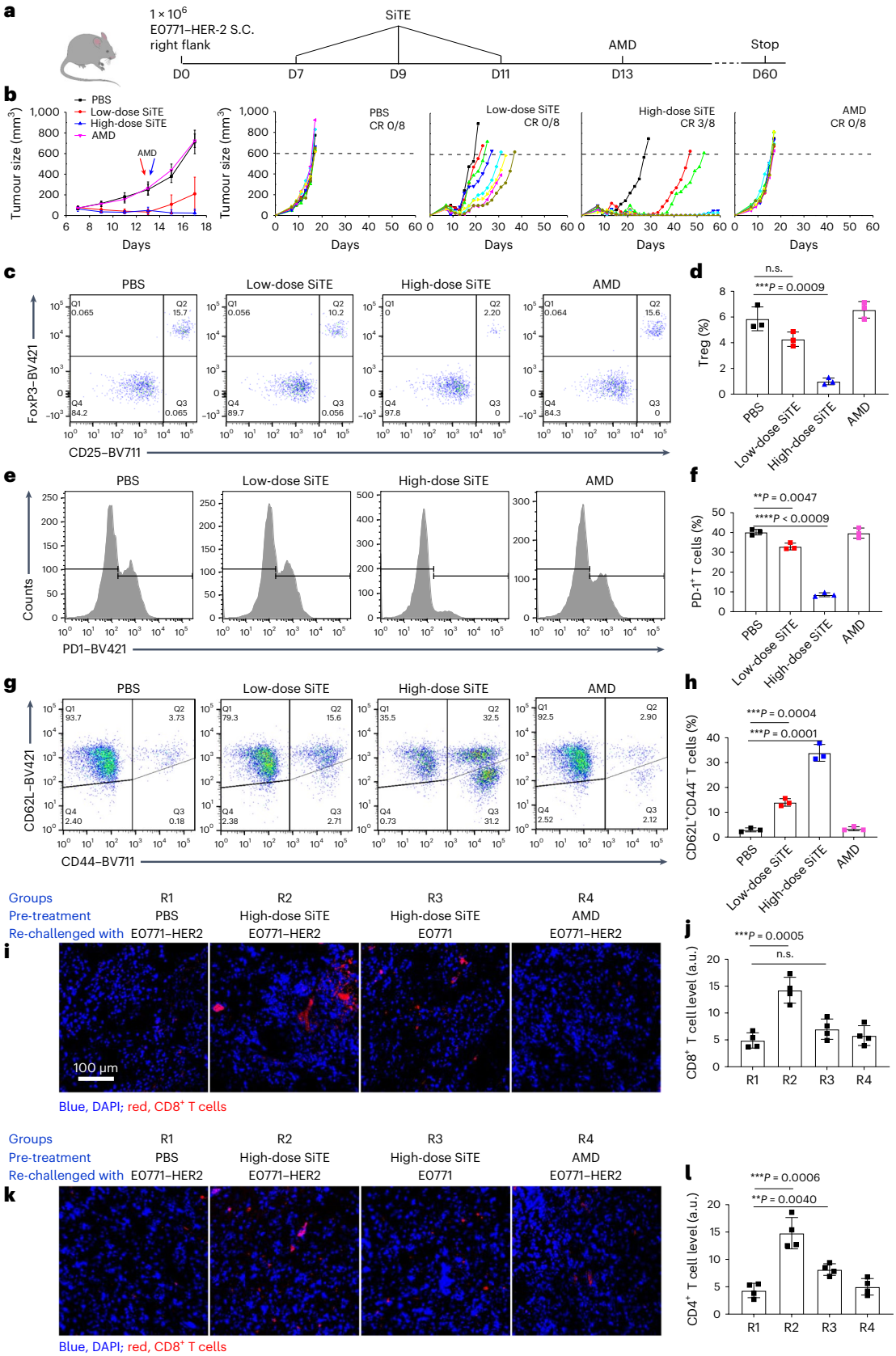

https://doi.org/10.1038/s41551-023-01147-6

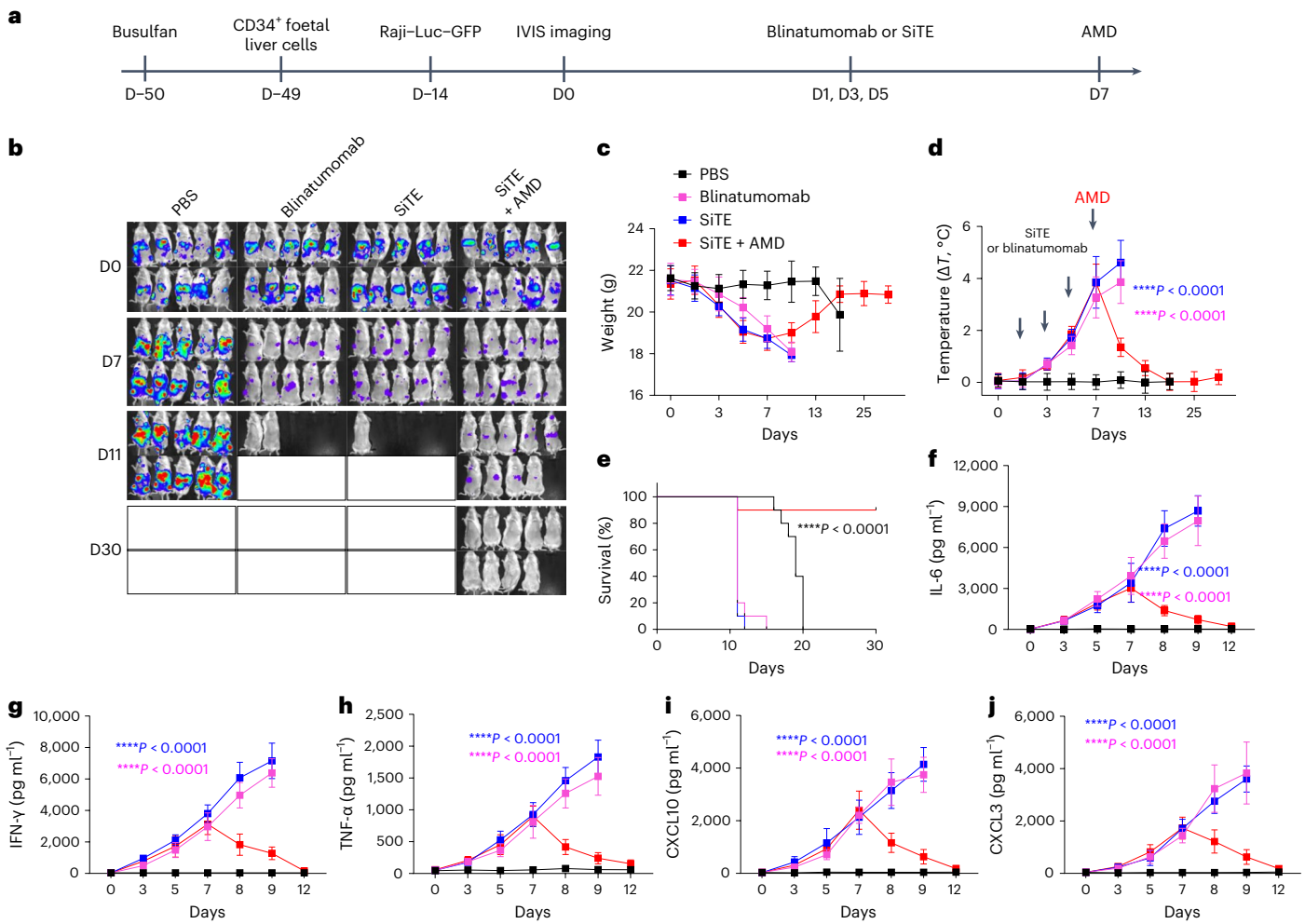

Fig. 6 | AMD reduces SiTE-induced CRS in vivo. a, NSG-SGM3 mice were treated with busulfan at day −50 (D−50) to remove the bone marrow. At day −49, 10^5 human CD34$^+$ foetal liver cells were i.v. injected to allow the mouse to develop a human immune system. Then, 10^6 Raji–Luc–GFP tumour cells were i.v. injected at day −14. At days 1, 3 and 5, PBS, blinatumomab (5 mg kg^{-1}) or SiTE (5 mg kg^{-1}) was i.v. injected. When an approximate 15% decrease in body weight (indicative of toxicity) was observed on day 7, half of the mice that had received SiTE were given an i.v. injection of AMD. Throughout the study, mice were euthanized when body weight decreased more than 20%. IVIS was used to monitor tumour burden in vivo. **b**, IVIS images of the mice at days 0, 7, 10 and 30. **c**–**e**, Mouse body weight (**c**), temperature (**d**) and survival curves (**e**), $n = 10$ mice. The red stars in **b** and **c** indicate that mice were euthanized. **f**–**j**, Measurements of markers for CRS including IL-6 (**f**), IFN-γ (**g**), TNF-α (**h**), CXCL10 (**i**) CCL3 (**j**) levels in mouse blood at different timepoints, $n = 10$ mice. The data in **c**, **d** and **f**–**j** are plotted as mean ± s.d. ($n = 10$) from three independent experiments. *P* values are indicated in **d** and **f**–**j**. Blue, SiTE versus SiTE + AMD at day 9; pink, blinatumomab versus SiTE + AMD at day 9, analysed by two-tailed unpaired Student's *t*-tests. The *P* value in **e** was determined using the log-rank (Mantel–Cox) test.

used flow cytometry to determine T cell infiltration levels in liver tissue before and after AMD infusion. We found that treatment with SiTE greatly increased the number of T cells in liver tissue (Supplementary Fig. 20a–c). However, infusion of AMD after SiTE treatment greatly decreased the number of T cells in liver tissue (Supplementary Fig. 20b,c). Histology experiments further confirmed that SiTE caused severe liver cell damage, and AMD reversed this damage by decreasing T cell infiltration in the liver (Fig. 4i,j and Supplementary Fig. 21). These results demonstrate that the on-target off-tumour toxicity of SiTE can be controlled via AMD administration.

High doses of SiTE elicit a tumour-specific immune response with limited on-target off-tumour toxicity

We demonstrated that the off-tumour toxicity of SiTE can be controlled via an infusion of AMD to disassemble SiTE. However, although SiTE allieviated on-target, off-tumour toxicity, most tumours relapsed after treatment with an AMD infusion (Supplementary Fig. 22). This is due to AMD disassembling the SiTE and thus breaking the engagement of T cells and tumour cells. However, a key advantage of SiTE is their controllable activity to prevent off-tumour toxicity, which allows us to explore the use of higher doses of SiTE in further in vivo experiments. We constructed the E0771–HER2 mouse model with liver expression of human HER2 antigen. After the tumour size reached ~100 mm^3, we treated mice with PBS, a low dose of SiTE (1 mg kg^{-1}), a high dose of SiTE (5 mg kg^{-1}) or AMD (in 5% polyoxyethylene castor oil) only (Fig. 5a). When mouse body weight decreased by more than 15%, AMD was administered to decrease the off-tumour toxicity (Extended Data Fig. 4a). As shown in Fig. 5b, in mice treated with PBS, the tumours reached 600 mm^3 at around day 17 and mice were euthanized. In mice that received the low dose of SiTE, tumour growth was inhibited through day 13 when AMD was administered. However, most tumours continued to grow after the infusion of AMD to disassemble SiTE, and no mice in this group survived past day 60 (Fig. 5b). In mice treated with the high dose of SiTE, tumour growth was greatly inhibited through day 13, and after receiving AMD, only three of eight mice showed tumour relapse through day 60, with the majority of tumours remaining undetectable (Fig. 5b). Thus, the higher dose of SiTE allowed for continued anti-tumour activity in mice even after SiTE disassembly.

To better characterize this anti-tumour activity, we next performed an additional animal experiment to analyse the immune microenvironment in tumour tissue. Using the same E0771–HER2 model and treatment groups detailed above, mice were euthanized at day 17 and tumour tissue was isolated. Flow cytometry results showed that the $CD25^+FoxP3^+$ regulatory T cell (Treg) population (Fig. 5c,d) and $PD1^+$ exhausted T cells (Fig. 5e,f) were greatly decreased in mice treated with a high dose of SiTE. However, mice treated with a low dose of SiTE showed only a slight decrease in these cell populations (Fig. 5c–f). We also found that mice treated with a high dose of SiTE greatly increased both $CD44^+CD62L^+$ central memory cells and $CD44^+CD62L^-$ effector memory cell populations in tumour tissue (Fig. 5g,h and Extended Data Fig. 4c). Moreover, the increased expression of co-stimulatory molecules, such as CD40, CD80 and CD86 on dendritic cells (DCs) (Extended Data Fig. 5a–c), and higher HER2-specific total immunoglobulin (Ig)G, IgG2c and IgG1 levels were also detected in the high-dose SiTE group (Extended Data Fig. 5d–f). To investigate this prolonged anti-tumour activity, we performed a tumour cell rechallenging experiment (Extended Data Fig. 6). We injected 10^6 E0771–HER2 or E0771 cells into tumour-free mice from the high-dose SiTE group, and PBS or AMD pre-treated mice challenged with E0771–HER2 cells were used as controls. In mice that had previously received a high dose of SiTE and were challenged with E0771–HER2, only three of eight mice showed tumour growth, and tumour growth was much slower than in naive mice. Notably, when mice previously receiving high-dose SiTE were challenged with HER2-negative E0771, tumour growth was also inhibited, as only four of eight mice showed tumour growth and the other mice were tumour free (Extended Data Fig. 6d). This demonstrates that tumour-specific immune memory was induced after treatment with a high dose of SiTE. However, PBS or AMD pre-treated mice did not show any ability to inhibit tumour cell growth in this re-challenge model. To further explore the anti-tumour activity in SiTE-treated mice, we then analysed immune cell infiltration in the tumour tissue (Fig. 5i–l and Extended Data Fig. 6f–h). The results demonstrated that T cells readily infiltrated into tumour tissue in mice previously treated with SiTE. Most of the $CD3^+$ T cells were PD1 negative in mice that had received a high dose of SiTE, and Treg cell number was also decreased in these mice compared with the $CD3^+$ T cells in mice receiving no SiTE treatments (Extended Data Fig. 6f–h, flow gating strategies are shown in Supplementary Fig. 23).

To better understand how the high dose of SiTE induces an in situ vaccination effect, we performed two additional experiments. We found that inactivation of tumour cells with formaldehyde before injection into mice and treating the mice with high doses of SiTE and AMD failed to provide the mice protection from both E0771 and E0771–HER2 cell rechallenging (Supplementary Fig. 24). Moreover, we found that T cells isolated from high-dose SiTE-treated mice induced modest target tumour cell killing, compared with T cells isolated from PBS-treated mice (Extended Data Fig. 7a). Moreover, an in vivo killing assay demonstrated that high-dose SiTE elicited a tumour cell-specific immune response (Extended Data Fig. 7b,c). These results further support the contribution of the in situ vaccination effect in tumour growth inhibition and long-term protection. Additionally, we found that high doses of SiTE induced the release of higher levels of damage-associated molecular patterns (DAMPs) from the tumour cells (Extended Data Fig. 8a). Moreover, increased release of HER2 antigen and many mutation-derived neoantigens were also detected (Extended Data Fig. 8b,c). These DAMPs and antigens can be taken up by DCs and tumour antigen-specific T cell immune responses can be elicited[54,55]. This can not only recognize HER2-positive E0771 cells, but can recognize the HER2-negative E0771 cells because of the shared neoantigen expression in both E0771 and E0771–HER2 cell lines. These results demonstrate that a high dose of SiTE elicited an in situ vaccination effect that can provide protection from tumour relapse.

SiTE decrease CRS and neurotoxicity in a humanized immune system mice model

Since we have demonstrated that the SiTE strategy can be used to control the on-target off-tumour toxicity in a mouse HER2 tumour model, we investigated whether this strategy can be used to control CRS and neurotoxicity. CRS and neurotoxicity models were constructed in a humanized immune system mouse model when using CAR T cells to treat B cell lymphoma[56]. In our study, we investigated whether the SiTE that targets human CD3 and human CD19 can be used to control on-target off-tumour toxicity, CRS and neurotoxicity in the humanized immune system mouse model.

We first constructed a humanized immune system mouse model by transplanting human $CD34^+$ foetal liver cells into busulfan-treated mice (Supplementary Fig. 25). Next, we expressed human CD19 protein in the livers of these mice using a piggybac transposon system at day −35 (Supplementary Fig. 26). Raji cells, a human Burkitt's lymphoma cell line, were i.v. injected to construct the tumour model at day −14 (Supplementary Fig. 25). The Raji cells also express luciferase and green fluorescent protein (GFP) as reporters (Raji–Luc–GFP) so that we can monitor the tumour and its growth in vivo. We found that treatment with either blinatumomab or SiTE not only induced on-target off-tumour toxicity in the liver, but led to strong CRS (Fig. 6, Supplementary Fig. 33 and Extended Data Fig. 9). The levels of cytokines such as IL-6 and TNF-α were similar in blinatumomab- and SiTE-treated mice (Supplementary Fig. 25). Tocilizumab is a commercialized drug for CRS treatment in the clinic, and has been shown to prevent CRS in a humanized mouse model by preventative administration[56]. Thus, to solely evaluate the effect of on-target off-tumour toxicity, we administered tocilizumab before either blinatumomab, SiTE or PBS was i.v. injected as treatment (Extended Data Fig. 9a). Mouse body weight, serum cytokines and liver enzymes were monitored. Tumour burden was also monitored using IVIS. As shown in Extended Data Fig. 9b, both blinatumomab and SiTE treatment induced effective tumour cell killing. However, mouse body weight loss and liver enzyme release to the blood were also observed in these groups (Extended Data Fig. 9c,e,f). When >15% body weight loss (day 7) was observed, mice in the SiTE group were i.v. injected with AMD. We found that AMD treatment greatly decreased the liver enzyme levels and cytokine levels in blood (Extended Data Fig. 9e–h), indicating that on-target off-tumour toxicity had been controlled. However, if left untreated, blinatumomab and SiTE treatment induced greater toxicity and ultimately led to mouse death (Extended Data Fig. 9d). Histology analysis also confirmed that AMD can suppress the off-tumour toxicity caused by SiTE (Extended Data Fig. 9i,j).

Although AMD treatment inhibited SiTE activity, no tumour cells were detected at day 30 (Extended Data Fig. 9b). To investigate whether the tumour cell clearance was a result of tumour-specific immune response, we rechallenged the tumour-free mice from the SiTE + AMD group with 10^6 Raji–Luc–GFP cells, and tumour burden over time was monitored (Extended Data Fig. 9k). We found that Raji–Luc–GFP cells were quickly cleared from the mice, demonstrating that the SiTE + AMD treatment induced an immune memory effect towards the tumour cells. To further confirm that SiTE + AMD treatment induced a tumour-specific T cell response, T cells in the tumour-free mice from the SiTE + AMD group were sorted and co-cultured with Raji–Luc–GFP cells for 24 h. Tumour cell viability and IFN-γ levels in the cell culture medium were determined. The results (Extended Data Fig. 9l,m) showed that T cells in the tumour-free mice from the SiTE + AMD group induced substantial tumour cell lysis and IFN-γ release (Extended Data Fig. 9k–m). These results demonstrate that SiTE can not only clear the tumour cells in the NSG mice, but they also induce lower off-tumour toxicity than blinatumomab, which eventually led to extended mouse survival.

We also compared SiTE with blinatumomab in treating symptoms of CRS and neurotoxicity. We constructed the humanized mouse model as before, but this time did not use the piggybac transposon system

to express CD19 in the mouse liver. This allows us to better analyse the effect of the SiTE on CRS and neurotoxicity (Fig. 6a). Raji–Luc–GFP cells were i.v. injected at day −14. Blinatumomab, SiTE or PBS were i.v. injected into the mice at day 1. Mouse tumour burden, body weight, temperature and plasma cytokine levels were monitored (Fig. 6b–j). As shown in Fig. 6b–e, both the SiTE and blinatumomab treatments induced high fever and body weight loss shortly after treatment. Further, plasma cytokine levels showed that IL-6, IFN-γ, TNF-α, CXCL10 and CCL3 concentrations greatly increased after both the SiTE and blinatumomab treatments (Fig. 6f–j). At the first sign of toxicity (high fever, $\Delta T > 2$ °C) in the SiTE-treated mice, 10 mg kg^{-1} AMD was i.v. injected into mice. Notably, the body weight loss and high fever was contained in the AMD-treated group 24 h after the treatment (Fig. 6c,d). Moreover, the increased cytokine levels gradually recovered to within normal ranges 24 h post-AMD treatment (Fig. 6f–j). However, mice treated with blinatumomab or SiTE alone presented with higher fever and increased weight loss at day 9, which eventually led to mouse death (Fig. 6e). Although AMD treatment inhibited the anti-tumour activity of SiTE, tumour cells were not detected at day 30 (Supplementary Fig. 6b). This is because of the tumour-specific immune response generated by the high-dose SiTE treatment, as demonstrated in Supplementary Fig. 35k–m. These results demonstrate that the SiTE strategy can suppress CRS and prolong survival in a humanized immune system mouse model bearing the human CD19 B cell lymphoma.

We also evaluated whether the SiTE can help control neurotoxicity. In the clinic, neurotoxicity is usually delayed and occurs several weeks after CRS onset. Tumour-bearing mice were treated with SiTE at days 1, 3 and 5 (Extended Data Fig. 10a). Tocilizumab or AMD were used when signs of CRS presented (high fever, $\Delta T > 2$ °C). In this way, we can greatly inhibit the symptoms of CRS and prolong mouse survival to evaluate the effect of the SiTE on neurotoxicity. Rather than use a preventative strategy for treating CRS (Extended Data Fig. 9), here we used Tocilizumab to treat CRS when symptoms presented, so that we can compare it directly with our SiTE strategy. As shown in Extended Data Fig. 10b, tumour-bearing NSG-SGM3 mice displayed increased body weight loss after SiTE treatment. One group was treated with tocilizumab, and the other group was treated with AMD. Mouse body weight and temperature gradually recovered to normal ranges after both the tocilizumab and AMD treatments. AMD treatment decreased both levels of IL-6 and IL-1 cytokines in mouse blood, while tocilizumab did not (Extended Data Fig. 10d,e). This is consistent with previous studies since tocilizumab is an antibody for the IL-6 receptor so it will not decrease IL-6 concentration in blood[57]. At around day 33, mice that received tocilizumab developed sudden paralysis (Extended Data Fig. 10g) or seizure (Extended Data Fig. 10h), which are signs of lethal neurological syndrome. However, most mice in the AMD group did not develop these symptoms. Studies have shown that IL-1 is the major cause of neurotoxicity[56]. We speculate that the AMD-induced protection from neurotoxicity is due to the rapid recovery of IL-1 levels back to normal physiological ranges. In mice that developed paralysis and seizure in the tocilizumab treatment group, mice did show brain meningeal thickening (Extended Data Fig. 10i) accompanied by human monocyte infiltration in the subarachnoid space, as determined by immunohistochemistry analysis of human CD68 (Extended Data Fig. 10j). Brain meningeal thickening and human monocyte infiltration were not observed in mice treated with AMD. Moreover, prolonged animal survival (Extended Data Fig. 10f) in the AMD treatment group was observed. These results demonstrate that the SiTE strategy can also protect mice from lethal neurotoxicity.

After demonstrating that SiTE is advantageous over blinatumomab in terms of lower on-target off-tumour toxicity, lower CRS and neurotoxicity, we also compared the anti-tumour efficacy of SiTE and Blinatumomab in vivo. To specifically assess the anti-tumour efficacy of blinatumomab and SiTE, we refrained from expressing the CD19 antigen in the mouse liver. By employing this approach, we ensured that treatment with either blinatumomab or SiTE would not elicit on-target off-tumour toxicity. To further avoid the effect of CRS on the evaluation of the therapeutic outcome of blinatumomab and SiTE, we employed normal NSG mice, devoid of humanization. Our study shows that both blinatumomab and SiTE induced substantial suppression of tumour growth (Supplementary Fig. 27b,c). Remarkably, at day 13, the tumour burden exhibited a notably lower level in mice treated with SiTE in comparison to those treated with blinatumomab (Supplementary Fig. 27b,c), thereby emphasizing the anti-tumour efficacy of SiTE.

We also investigated whether Blinatumomab could also induce a vaccine effect. We found that high-dose blinatumomab induced substantial release of DAMPs and tumour antigens from tumour cells (Supplementary Fig. 28a,b). Since high levels of DAMPs and tumour antigen release have been demonstrated to improve antigen processing and presentation[58], it is highly possible that high-dose blinatumomab can also induce an in situ vaccine effect. To demonstrate the vaccine effect in vivo, we collected T cells from mice treated with a high dose of blinatumomab and cultured them with Raji–Luc–GFP tumour cells. We found that the T cells induced substantial tumour cell killing compared with T cells collected from PBS-treated mice (Supplementary Fig. 28c). These results demonstrate that high-dose blinatumomab can also induce a vaccine effect. We also delved into the question of whether CRS could be halted by simply discontinuing the administration of blinatumomab, owing to its inherent short half-life. Our results (Supplementary Fig. 29a–c) showed that mice treated with blinatumomab developed of CRS, characterized by a notable elevation of IL-6 levels within the serum (Supplementary Fig. 29b). Notably, this surge in IL-6 persisted and ultimately led to the mortality of the mice, even after cessation of blinatumomab treatment (Supplementary Fig. 29c). Even though blinatumomab possesses a short serum half-life, the accumulation within tumour tissues and normal tissues expressing CD19 can persist for a longer time (Supplementary Fig. 14d). The pronounced targeting of T cells and CD19-expressing cells, coupled with heightened activation of many immune cells, served to amplify the cytokine cascade, rendering it impervious to interruption by the mere discontinuation of blinatumomab usage. These findings underscore the critical need for the development of an alternative to blinatumomab—one that can be switched off as needed—in this rapidly evolving research field.

Outlook

Cancer immunotherapy using BiTEs has shown great promise in the clinic, as it can engage T cells and tumour cells while activating T cells to lyse tumour cells. In this study, we prepared a SiTE for potent cancer immunotherapy with an 'off' switch. Whereas the off-tumour toxicity induced by traditional BiTEs is difficult to control, SiTE is designed to disassemble when exposed to the small molecule AMD because of the higher affinity of β-CD and AMD compared with phenyl. SiTE may serve as a broad delivery technique for future bispecific antibody designs for cancer immunotherapy while avoiding the risks of toxicity. Considering the variability of the pharmacokinetics and pharmacodynamics of AMD and SiTE once they are administered to humans, optimization of the dose and timepoints of AMD to be given to each cancer patient will be challenging. A potential risk of this SiTE is that it might induce T cell crosslinking and cytokine release because random rather than site-specific conjugation of PEG-phenyl and PEG-β-CD to CD3 and HER2 antibodies were used for all experiments in this work. Our strategic approach involves the incorporation of recombinant CD3 and CD19/HER2 Fab fragments equipped with engineered C-terminal conjugation sites, thereby enabling site-specific conjugation. This will facilitate the construction of SiTE boasting uniform structure, for instance, a singular CD3 Fab molecule conjugated to a singular HER2 Fab molecule via supramolecular interactions. This enables the evolution to our next generation of SiTEs. We believe that this advancement will enhance the viability and manufacturability of our approach and lead to diminished batch-to-batch variability, thus greatly bolstering its suitability for

clinical translation. We believe that SiTE may be a promising strategy for developing effective and safe cancer immunotherapies.

Methods

Materials

Chemicals and antibodies: anti-human HER2 (cat. no. BE0277, clone: 7.16.4), anti-mouse CD3 (cat. no. BE001-1FAB, clone: 145-2C11 f(ab')2 Fragments) and anti-human CD3 (cat. no. BE0231, clone: UCHT1 (Leu-4) (T3)) antibodies were purchased from BioXcell. Flow antibodies anti-mouse CD45–Brilliant Violet 421 (cat. no. 103133, clone: 30-F11, 1:100 dilution), anti-mouse CD3–PE (cat. no. 100206, clone: 17A2,1:100 dilution), anti-mouse CD4–Alexa Fluor 488 (cat. no. 100423, clone: GK1.5,1:100 dilution), anti-mouse CD8–APC (cat. no. 100712, clone: 53-6.7, 1:100 dilution), anti-mouse FoxP3–Brilliant Violet 421 (cat. no. 126419, clone: MF-14, 1:100 dilution), anti-mouse CD25–Brilliant Violet 711 (cat. no. 102049, clone: PC61, 1:100 dilution), anti-mouse CD44–Brilliant Violet 421 (cat. no. 103039, clone: IM7, 1:100 dilution), anti-mouse CD62L–Brilliant Violet 711 (cat. no. 104445, clone: MEL-14, 1:100 dilution) were purchased from Biolegend. NH_2–PEG2000–MAL was obtained from Creative PEGWorks. β-CDs and 3-phenylpropanoyl chloride were obtained from Sigma. The mouse IgG1 Fab kit was ordered from New England Biolabs (cat. no. P0770S). The mouse IgG2a Fab purification kit was ordered from Thermo Fisher (cat. no. 44985). The piggyBac transposase vector pCMV–hyPBase and the pPB7 TBG. human HER2.P2A.IRFP720 plasmids that were used to construct the HER2 expression model was a gift from the laboratory of Dr. Carl June.

Cell lines

E0771 and E0771–HER2 cells were requested from Dr Betty Y. S. Kim. Raji–Luc–GFP cells were requested from Dr Alan Epstein. All of the cell lines tested negative for mycoplasma at the University of Pennsylvania cell center.

Animals

C57BL/6 mice (female, 6–8 weeks old) were ordered from the Jackson laboratory and housed in a specific-pathogen-free animal facility at ambient temperature (22 ± 2 °C), air humidity 40–70% and 12 h dark/12 h light cycle. NSG-SGM3 mice (female, 6–8 weeks old) were ordered from the Jackson laboratory. For IVIS imaging, an alfalfa- and fenbendazole-free mouse diet was used to decrease the background fluorescence signal. All protocols performed on animals in this study were approved by the institutional animal care and use committee of the University of Pennsylvania.

Antibody Fab fragment preparation

The Fab fragments of anti-mouse CD3 and anti-human HER2 antibodies were prepared using commercialized Fab preparation kits following the manufacturers' manuals.

Modifying CD3 and HER2 Fabs with 2-iminothiolane

There are only two thiol groups on each Fab fragment. We increased the number of thiol groups on the fragments using a reported method[35]. To prepare the thiol-modified antibody fragments, 2-iminothiolane was added to 500 μg of antibody fragment and the mixture was incubated at 37 °C for 4 h. Free 2-iminothiolane was removed using a centrifugal filter (molecular weight cut off (MWCO) of 3 kDa). The free thiol groups on the antibody Fabs before and after 2-iminothiolane modification were measured using a commercialized free thiol assay kit (ab112158). Since we know that each unmodified Fab contains 2 free thiol groups after mild reduction, we calculated the total thiols on each antibody fragment (N) using the following equation:

N = (total thiol groups after 2-iminothiolane modification/total thiol groups before 2-iminothiolane modification) × 2

We found that, on average, 4.7 and 4.9 thiol groups were added to the CD3 Fab and HER2 Fab, respectively.

Preparation of the SiTEs

We first prepared PEG-phenyl and PEG-β-CD conjugations. For CD3 Fab–PEG-phenyl1 synthesis, the anti-CD3 Fab was mixed with MAL–PEG-phenyl at a 1:1 ratio in PBS for 2 h with gentle stirring at room temperature, then unconjugated MAL–PEG-phenyl or MAL–PEG-β-CD were removed using a centrifugal filter with a MWCO of 10 KDa. After washing with PBS several times, the antibody Fab–PEG-phenyl or Fab–PEG-β-CD was stored at 4 °C for future applications. CD3 Fab–PEG-phenyl2, CD3 Fab–PEG-phenyl3 and CD3 Fab–PEG-phenyl4 were synthesized using the same protocol except a 1:2, 1:3 or 1:4 ratio of CD3 Fab to MAL–PEG-phenyl was used, respectively. HER2 Fab–PEG-β-CD1, HER2 Fab–PEG-β-CD2 and HER2 Fab–PEG-β-CD3 were synthesized with similar steps except a 1:1, 1:2, 1:3 or 1:4 ratio of HER2 Fab and MAL–PEG-β-CD was used, respectively.

Quantification of the composition of SiTEs

The compositions of SiTEs were determined using a two-step separation and quantification method. To quantify the composition of each SiTE, SiTEs were firstly loaded on a centrifugal filter device with MWCO of 50 kDa to separate all free Fabs. To ensure the complete separation of free Fabs, SiTEs were washed two times with 1× PBS. The three elutes (contain free Fab) were combined and stored for quantification. The Fab clusters that cannot pass through the 50 kDa filter were collected and loaded on a centrifugal filter device with MWCO of 100 kDa. With similar steps, Fab dimers (molecular weight (MW) 50–100 kDa) were collected. Fab clusters that cannot pass through the 100 kDa filter were collected and loaded on a centrifugal filter device with MWCO of 300 kDa and Fab clusters with MW from 100 to 300 kDa were collected. The Fab clusters that cannot pass through the 300 kDa filter were collected and loaded on a centrifugal filter device with MWCO of 1,000 kDa. The Fab clusters with MW in the range of 300–1,000 kDa were collected. The Fab clusters that cannot pass through the 1,000 kDa were also collected. We found that these are mostly nanoparticles when observed under TEM. The various components were quantified using bicinchoninic acid assay and their relative percentage was calculated.

Stability of SiTEs in the present of AMD, phenylalanine or tyrosine

Ten μg of SiTEs 1–4 were incubated with 500 μg AMD, 500 μg phenylalanine or 500 μg tyrosine at 37 °C for 2 h, then the components in the sample were analysed using the two-step separation and quantification method as mentioned above.

SEC and circular dichroism

SEC experiments were performed using 100 μl injections with a Superose 6 Increase 10/300 column at 0.5 ml min^{-1} at 25 °C. The mobile phase consisted of 20 mM TrisHCl buffer (pH 7.4) containing 150 mM NaCl, filtered with 0.22 μm nylon membrane and degassed.

Circular dichroism experiments were performed on an Aviv 202 Circular Dichroism system. Antibody samples were dissolved in pure water and loaded in 1 cm quartz cells at room temperature. The spectra were recorded over a wavelength range 200–240 nm at sample concentration of 0.2 mg ml^{-1} at 20 °C. The final spectra were the average of 20 scans. CD spectra of the buffer solutions in the appropriate cuvette were subtracted from the sample spectra as background.

FRET experiment

CD3 Fab–PEG-phenyl and HER2 Fab–PEG-β-CD were labelled with e450 and flourescein isothiocyanate (FITC), respectively. For a typical synthesis, 100 μg of CD3 Fab–PEG-phenyl was mixed with 5 nmol of e450 in PBS buffer at room temperature under gentle stirring. After 2 h, the mixture was collected and dialyzed against PBS for 48 h. FITC-labelled HER2 Fab–PEG-β-CD was prepared with similar steps except FITC was used. The photoluminescence spectrum of the e450-labelled CD3 Fab–PEG-phenyl, FITC-labelled HER2 Fab–β-CD and the mixture of these

two molecules were measured on a HORIBA FluoroMax-3 fluorescence spectrometer with excitation wavelength of 405 nm, and emission spectrum were collected from 420 to 700 nm.

Gel electrophoresis and DLS

Protein samples were loaded on the polyacrylamide basic native gel (4–12%). The running conditions were as follows: 120 V, 45 min. 2-(N-morpholino)ethanesulfonic acid (MES)-sodium dodecyl sulfate (SDS) buffer was used. For DLS, SiTEs with concentrations of 50 μg ml^{-1} were used and the data was collected on a Malvern Zetasizer Nano machine.

Generation of primary mouse T cells

Primary mouse T cells were isolated from the spleens of 6-week-old female C57BL/6 mice[59]. After mice were euthanized, the spleens were collected, cut into pieces and homogenized on a 100 μm cell strainer. Then, red blood cells were lysed with ammonium–chloride–potassium lysing buffer and the cell suspensions were passed through a 70 μm cell strainer. CD3$^+$ T cells were collected using a STEMCELL T cell isolation kit resulting in approximately 2×10^7 CD3$^+$ T cells obtained from each mouse spleen.

Ex vivo killing assays

The target cells, E0771–HER2 or E0771 that express a luciferase reporter were incubated with primary mouse CD3$^+$ T cells with different treatments. After 24 h, target cell viability was measured by determining the luciferase expression level using a luciferase assay kit. In additional assays, Raji cells were tagged with both GFP and luciferase, and the viability of Raji cells was monitored using a luciferase assay kit.

Quantification of cell-to-cell interactions

E0771–HER2 cells were labelled with carboxyfluorescein succinimidyl ester (CFSE)-green and primary T cells were labelled with CFSE-red. The two cells were co-cultured and then treated with PBS or SiTE for 2 h. After that, the cells were observed by confocal imaging. T cell to T cell interactions and T cell to tumour cell interactions were counted manually by taking ten images for quantification.

Determination of cytokine concentrations and liver enzymes

Mouse blood was collected at different timepoints and the serum was obtained by centrifuging the clotted blood. Cell culture medium was collected at different timepoints. For the detection of various cytokines in cell culture medium or mouse serum, 100 μl of medium or serum was used for each sample and the cytokines (IL-6, IL-1, IFN-γ, TNF-α, CXCL10 or CCLS) were detected using either enzyme-linked immunosorbent assays kits or a FirePlex-96 Key Cytokines Immunoassay Panel (cat. no. ab243549) following the manufacturers protocol. Mouse serum was collected and the ALT and AST levels were detected using an alanine transaminase colorimetric activity assay kit (cat. no. 700260, Cayman) or an aspartate aminotransferase colorimetric activity assay Kit (cat. no. 701640, Cayman).

QCM

Gold-coated QCM-D sensors with a resonance frequency of 4.95 MHz were cleaned using a plasma cleaner and then rinsed with PBS. A Q-Sense E4 QCM-D system was used to monitor the shifts in the resonance frequency (ΔF) and dissipation (ΔD) for odd overtones ($n = 1$, 3, …13). CD3 or HER2 protein was adsorbed on the gold-coated sensor by flowing 0.2 mg ml^{-1} CD3 or HER2 in PBS over the crystals. After ~10 min of adsorption, the CD3 or HER2 layers were rinsed with PBS until equilibration was achieved (~15 min). Interactions between free CD3 Fab or SiTE and CD3 protein were measured by flowing 200 μg ml^{-1} CD3 Fab or SiTE in PBS over the adsorbed CD3 protein layer. Interactions between free HER2 Fab or SiTE and HER2 protein were tested by flowing 200 μg ml^{-1} HER2 Fab or SiTE in PBS over the adsorbed HER2 protein layer. PBS buffer was introduced using continuous pumping after about 50 min of adsorption of the nanoparticles onto the antigen layer. Control measurements were performed by flowing free CD3 or HER2 Fab solutions over clean gold-coated sensors until the frequency change had plateaued, then the CD3 or HER2 Fab-adsorbed surface was rinsed with PBS to remove any free antibody fragments.

Binding-avidity assay

Binding affinity of antibodies to their target proteins was determined using a reported method[39]. The HER2-overexpressing E0771–HER2 cells was cultured in 96-well cell culture plates and grown to approximately 80% confluence. The cells were then fixed with 4% formaldehyde and incubated with various concentrations of SiTE (labelled with FITC) and blocked with bovine serum albumin for 30 min. Unbound SiTE was then removed with three washes of PBS. Absorbance was measured at 488 nm, with non-fluorescently labelled SiTE used as a control. The dissociation constant K_d was obtained by plotting normalized absorbance values versus concentrations of the SiTE added to the cell cultures. To measure the K_d for CD3 Fab binding to CD3 antigen and SiTE binding to CD3 antigen, we firstly coated the 96-well plates using retronectin to make the T cells adhere to the plates. Then, the K_d of free CD3 Fab to CD3 antigen and SiTE to CD3 antigen were determined using similar experiments as described above.

Flow experiments

Mice were euthanized with CO_2 and perfused with a 37 °C PBS buffer containing collagenase IV (0.5 mg ml^{-1}), dispase (50 units ml^{-1}) and DNase (50 units ml^{-1}). After 30 min of digestion, the tumour tissue was cut into small pieces and homogenized on a 100 μm cell strainer. Then red blood cells were lysed with ACK lysing buffer and the cell suspensions were passed through a 70 μm cell strainer. One million cells were stained with different antibodies for 30 min and washed two times with PBS before analysis on the flow cytometer (LSR, BD).

Construction of the humanized immune system mice model

Recently, a study developed a humanized immune system NSG-SGM3 mouse model and found that when CAR T cells were infused to kill cancer cells, it can induce several major symptoms of human CRS and neurotoxicity[56]. Here, we constructed a humanized mouse model following their method with some modification. NSG-SGM3 mice were treated with busulfan (40 mg kg^{-1}) to remove the bone marrow, then 10^5 human foetal liver CD34$^+$ cells were i.v. injected to the mice. The development of human immune cells was confirmed after 5 weeks post-CD34$^+$ foetal liver cell infusion.

Construction of the mice model with human HER2 or CD3 expression in the liver

The June laboratory has reported a mouse model with stable expression of the human HER2 antigen in the liver[50]. They used a hydrodynamic injection method to deliver a piggyBac transposase vector pCMV–hyPBase and the pPB7 TBG.human HER2.P2A.IRFP720 plasmids to the mouse liver. Here, we modified this animal model construction and delivered the two plasmids with a MC3 LNP[52]. The LNPs were synthesized using a microfluidic device to mix an aqueous phase containing plasmids and an organic phase containing DLin-MC3-DMA cationic lipid, 1,2-distearoyl-sn-glycero-3-phosphocholine, C14-PEG2000 and cholesterol. The LNPs were dialyzed against PBS and passed through a 0.22 μm filter before use. LNPs were i.v. injected to mice at a dose of 2 μg plasmid per mouse. Human CD3 antigen was expressed in the liver of NSG-SGM3 mice using LNPs delivering pPB–CMV–hCD19:T2A:EGFP and pCMV–hyPBase plasmids.

Statistics

Graphpad prism 7.0 software was used to conduct statistical analysis. Error bars represent means ± s.d. Animal experiments were conducted

after randomization, and 7–8 mice were used in each group. A two-tailed Student's *t*-test was used to calculate the statistical differences between two groups. The differences in animal survival experiments were calculated using the Kaplan–Meier method, and the log-rank test was used to determine the *P* values.

Reporting summary

Further information on research design is available in the Nature Portfolio Reporting Summary linked to this article.

Data availability

The data supporting the results in this study are available within the paper and its Supplementary Information. The raw and analysed datasets generated during the study are available for research purposes from the corresponding authors on reasonable request. Source data are provided with this paper.

References

1. Huehls, A. M., Coupet, T. A. & Sentman, C. L. Bispecific T-cell engagers for cancer immunotherapy. *Immunol. Cell Biol.* **93**, 290–296 (2015).
2. Rader, C. Bispecific antibodies in cancer immunotherapy. *Curr. Opin. Biotechnol.* **65**, 9–16 (2020).
3. Weidanz, J. Targeting cancer with bispecific antibodies. *Science* **371**, 996–997 (2021).
4. de Miguel, M., Umana, P., de Morais, A. L. G., Moreno, V. & Calvo, E. T-cell-engaging therapy for solid tumors. *Clin. Cancer Res.* **27**, 1595–1603 (2021).
5. Tian, Z., Liu, M., Zhang, Y. & Wang, X. Bispecific T cell engagers: an emerging therapy for management of hematologic malignancies. *J. Hematol. Oncol.* **14**, 1–18 (2021).
6. Smits, N. C. & Sentman, C. L. Bispecific T-cell engagers (BiTEs) as treatment of B-cell lymphoma. *J. Clin. Oncol.* **34**, 1131 (2016).
7. Krishnamurthy, A. & Jimeno, A. Bispecific antibodies for cancer therapy: a review. *Pharmacol. Ther.* **185**, 122–134 (2018).
8. Duell, J. et al. Bispecific antibodies in the treatment of hematologic malignancies. *Clin. Pharmacol. Ther.* **106**, 781–791 (2019).
9. Przepiorka, D. et al. FDA approval: blinatumomab. *Clin. Cancer Res.* **21**, 4035–4039 (2015).
10. Kantarjian, H. et al. Blinatumomab versus chemotherapy for advanced acute lymphoblastic leukemia. *N. Engl. J. Med.* **376**, 836–847 (2017).
11. Labrijn, A. F., Janmaat, M. L., Reichert, J. M. & Parren, P. W. Bispecific antibodies: a mechanistic review of the pipeline. *Nat. Rev. Drug Discov.* **18**, 585–608 (2019).
12. von Stackelberg, A. et al. Phase I/phase II study of blinatumomab in pediatric patients with relapsed/refractory acute lymphoblastic leukemia. *J. Clin. Oncol.* **34**, 4381–4389 (2016).
13. Topp, M. S. et al. Safety and activity of blinatumomab for adult patients with relapsed or refractory B-precursor acute lymphoblastic leukaemia: a multicentre, single-arm, phase 2 study. *Lancet Oncol.* **16**, 57–66 (2015).
14. Fadul, C. et al. A phase I study targeting newly diagnosed glioblastoma with anti-CD3× anti-EGFR bispecific antibody armed T cells (EGFR BATs) in combination with radiation and temozolomide. *Brain Tumor Res. Treat.* **10**, S193 (2022).
15. Fiedler, W. et al. Phase I safety and pharmacology study of the EpCAM/CD3-bispecific BiTE antibody MT110 in patients with metastatic colorectal, gastric, or lung cancer. *J. Clin. Oncol.* **28**, 2573–2573 (2010).
16. Hutchings, M. et al. Glofitamab, a novel, bivalent CD20-targeting T-cell–engaging bispecific antibody, induces durable complete remissions in relapsed or refractory B-cell lymphoma: a phase I trial. *J. Clin. Oncol.* **39**, 1959–1970 (2021).
17. Heitmann, J. S. et al. Protocol of a prospective, multicentre phase I study to evaluate the safety, tolerability and preliminary efficacy of the bispecific PSMAxCD3 antibody CC-1 in patients with castration-resistant prostate carcinoma. *BMJ Open* **10**, e039639 (2020).
18. Lum, L. G. et al. Clinical and immune responses to anti-CD3 x anti-EGFR bispecific antibody armed activated T cells (EGFR BATs) in pancreatic cancer patients. *Oncoimmunology* **9**, 1773201 (2020).
19. Lum, L. G. et al. Phase II clinical trial using anti-CD3× anti-HER2 bispecific antibody armed activated T cells (HER2 BATs) consolidation therapy for HER2 negative (0–2+) metastatic breast cancer. *J. Immunother. Cancer* **9**, e002194 (2021).
20. Van De Vyver, A. J., Marrer-Berger, E., Wang, K., Lehr, T. & Walz, A.-C. Cytokine release syndrome by T-cell-redirecting therapies: can we predict and modulate patient risk? *Clin. Cancer Res.* https://doi.org/10.1158/1078-0432.CCR-21-0470 (2021).
21. Frey, N. V. & Porter, D. L. Cytokine release syndrome with novel therapeutics for acute lymphoblastic leukemia. *Hematol. Am. Soc. Hematol. Educ. Program* **2016**, 567–572 (2016).
22. Stein, A. S. et al. Neurologic adverse events in patients with relapsed/refractory acute lymphoblastic leukemia treated with blinatumomab: management and mitigating factors. *Ann. Hematol.* **98**, 159–167 (2019).
23. Parker, K. R. et al. Single-cell analyses identify brain mural cells expressing CD19 as potential off-tumor targets for CAR-T immunotherapies. *Cell* **183**, 126–142. e117 (2020).
24. Goebeler, M.-E. & Bargou, R. C. T cell-engaging therapies—BiTEs and beyond. *Nat. Rev. Clin. Oncol.* **17**, 418–434 (2020).
25. Gross, G. & Eshhar, Z. Therapeutic potential of T cell chimeric antigen receptors (CARs) in cancer treatment: counteracting off-tumor toxicities for safe CAR T cell therapy. *Annu. Rev. Pharmacol. Toxicol.* **56**, 59–83 (2016).
26. Kallioniemi, O.-P. et al. ERBB2 amplification in breast cancer analyzed by fluorescence in situ hybridization. *Proc. Natl Acad. Sci. USA* **89**, 5321–5325 (1992).
27. Morgan, R. A. et al. Case report of a serious adverse event following the administration of T cells transduced with a chimeric antigen receptor recognizing ERBB2. *Mol. Ther.* **18**, 843–851 (2010).
28. Morris, E. C., Neelapu, S. S., Giavridis, T. & Sadelain, M. Cytokine release syndrome and associated neurotoxicity in cancer immunotherapy. *Nat. Rev. Immunol.* **22**, 85–96 (2022).
29. Suurs, F. V., Lub-de Hooge, M. N., de Vries, E. G. & de Groot, D. J. A. A review of bispecific antibodies and antibody constructs in oncology and clinical challenges. *Pharmacol. Ther.* **201**, 103–119 (2019).
30. Bai, Y., Luo, Q. & Liu, J. Protein self-assembly via supramolecular strategies. *Chem. Soc. Rev.* **45**, 2756–2767 (2016).
31. Sakamoto, S. & Kudo, K. Supramolecular control of split-GFP reassembly by conjugation of β-cyclodextrin and coumarin units. *J. Am. Chem. Soc.* **130**, 9574–9582 (2008).
32. Friberg, G. & Reese, D. Blinatumomab (Blincyto): lessons learned from the bispecific T-cell engager (BiTE) in acute lymphocytic leukemia (ALL). *Ann. Oncol.* **28**, 2009–2012 (2017).
33. Hubsher, G., Haider, M. & Okun, M. Amantadine: the journey from fighting flu to treating Parkinson disease. *Neurology* **78**, 1096–1099 (2012).
34. Schmid, D. et al. T cell-targeting nanoparticles focus delivery of immunotherapy to improve antitumor immunity. *Nat. Commun.* **8**, 1–12 (2017).
35. McCall, M. J., Diril, H. & Meares, C. F. Simplified method for conjugating macrocyclic bifunctional chelating agents to antibodies via 2-iminothiolane. *Bioconjug. Chem.* **1**, 222–226 (1990).

36. Ding, Y.-F. et al. Host–guest interactions initiated supramolecular chitosan nanogels for selective intracellular drug delivery. *ACS Appl. Mater. Interfaces* **11**, 28665–28670 (2019).
37. Estrada, E., Perdomo-López, I. & Torres-Labandeira, J. J. Combination of 2D-, 3D-connectivity and quantum chemical descriptors in QSPR. Complexation of α-and β-cyclodextrin with benzene derivatives. *J. Chem. Inf. Comput. Sci.* **41**, 1561–1568 (2001).
38. Liu, L. & Guo, Q.-X. Novel prediction for the driving force and guest orientation in the complexation of α-and β-cyclodextrin with benzene derivatives. *J. Phys. Chem. B* **103**, 3461–3467 (1999).
39. Jiang, W., Kim, B., Rutka, J. T. & Chan, W. C. Nanoparticle-mediated cellular response is size-dependent. *Nat. Nanotechnol.* **3**, 145–150 (2008).
40. Yuan, H. et al. Multivalent bi-specific nanobioconjugate engager for targeted cancer immunotherapy. *Nat. Nanotechnol.* **12**, 763–769 (2017).
41. Selvin, P. R. The renaissance of fluorescence resonance energy transfer. *Nat. Struct. Biol.* **7**, 730–734 (2000).
42. Zhang, B. et al. Site-specific PEGylation of interleukin-2 enhances immunosuppression via the sustained activation of regulatory T cells. *Nat. Biomed. Eng.* **5**, 1288–1305 (2021).
43. Harris, J. M. & Chess, R. B. Effect of pegylation on pharmaceuticals. *Nat. Rev. Drug Discov.* **2**, 214–221 (2003).
44. Dreier, T. et al. T cell costimulus-independent and very efficacious inhibition of tumor growth in mice bearing subcutaneous or leukemic human B cell lymphoma xenografts by a CD19-/CD3-bispecific single-chain antibody construct. *J. Immunol.* **170**, 4397–4402 (2003).
45. Aoki, F. Y. & Sitar, D. S. Clinical pharmacokinetics of amantadine hydrochloride. *Clin. Pharmacokinet.* **14**, 35–51 (1988).
46. Kim, C., Agasti, S. S., Zhu, Z., Isaacs, L. & Rotello, V. M. Recognition-mediated activation of therapeutic gold nanoparticles inside living cells. *Nat. Chem.* **2**, 962–966 (2010).
47. Tonga, G. Y. et al. Supramolecular regulation of bioorthogonal catalysis in cells using nanoparticle-embedded transition metal catalysts. *Nat. Chem.* **7**, 597–603 (2015).
48. Tokumura, T. et al. Enhancement of bioavailability of cinnarizine from its β-cyclodextrin complex on oral administration with DL-phenylalanine as a competing agent. *J. Pharm. Sci.* **75**, 391–394 (1986).
49. Braegelman, A. S. & Webber, M. J. Integrating stimuli-responsive properties in host–guest supramolecular drug delivery systems. *Theranostics* **9**, 3017 (2019).
50. Castellarin, M. et al. A rational mouse model to detect on-target, off-tumor CAR T cell toxicity. *JCI Insight* **5**, e136012 (2020).
51. Kim, M. J. & Ahituv, N. in *Pharmacogenomics* (Innocenti, F. & van Schaik, R. H. N. eds) 279–289 (Springer, 2013).
52. Arteta, M. Y. et al. Successful reprogramming of cellular protein production through mRNA delivered by functionalized lipid nanoparticles. *Proc. Natl Acad. Sci. USA* **115**, E3351–E3360 (2018).
53. Zhang, Y., Sun, C., Wang, C., Jankovic, K. E. & Dong, Y. Lipids and lipid derivatives for RNA delivery. *Chem. Rev.* https://doi.org/10.1021/acs.chemrev.1c00244 (2021).
54. Min, Y. et al. Antigen-capturing nanoparticles improve the abscopal effect and cancer immunotherapy. *Nat. Nanotechnol.* **12**, 877–882 (2017).
55. Zhou, Q. et al. Mannose-derived carbon dots amplify microwave ablation-induced antitumor immune responses by capturing and transferring 'danger signals' to dendritic cells. *ACS Nano* **15**, 2920–2932 (2021).
56. Norelli, M. et al. Monocyte-derived IL-1 and IL-6 are differentially required for cytokine-release syndrome and neurotoxicity due to CAR T cells. *Nat. Med.* **24**, 739–748 (2018).
57. Chen, F. et al. Measuring IL-6 and sIL-6R in serum from patients treated with tocilizumab and/or siltuximab following CAR T cell therapy. *J. Immunol. Methods* **434**, 1–8 (2016).
58. Melero, I., Castanon, E., Alvarez, M., Champiat, S. & Marabelle, A. Intratumoural administration and tumour tissue targeting of cancer immunotherapies. *Nat. Rev. Clin. Oncol.* **18**, 558–576 (2021).
59. Di, S. et al. Combined adjuvant of poly I: C improves antitumor effects of CAR-T cells. *Front. Oncol.* **9**, 241 (2019).

Acknowledgements

M.J.M. acknowledges support from a United States National Institutes of Health Director's New Innovator Award (DP2 TR002776), a Burroughs Wellcome Fund Career Award at the Scientific Interface, an NSF CAREER Award (CBET-2145491) and the American Cancer Society (RSG-22-122-01-ET).

Author contributions

N.G. and M.J.M. conceived and designed the experiments. N.G., L.X., J.Q. and X.H. performed the experiments. N.G., L.X., J.Q., X.H. and R.E. analysed the data. N.G., M.J.M. and M.M.B. wrote and edited the manuscript. N.C.S. and C.H.J. provided materials and were involved in discussions of the work. M.J.M. supervised the project. All authors discussed the results and commented on the manuscript.

Competing interests

N.G. and M.J.M. have filed a patent application related to this study. The other authors declare no competing interests.

Additional information

Extended data is available for this paper at https://doi.org/10.1038/s41551-023-01147-6.

Supplementary information The online version contains supplementary material available at https://doi.org/10.1038/s41551-023-01147-6.

Correspondence and requests for materials should be addressed to Michael J. Mitchell.

Peer review information *Nature Biomedical Engineering* thanks Archana Thakur and the other, anonymous, reviewer(s) for their contribution to the peer review of this work. Peer reviewer reports are available.

https://doi.org/10.1038/s41551-023-01147-6

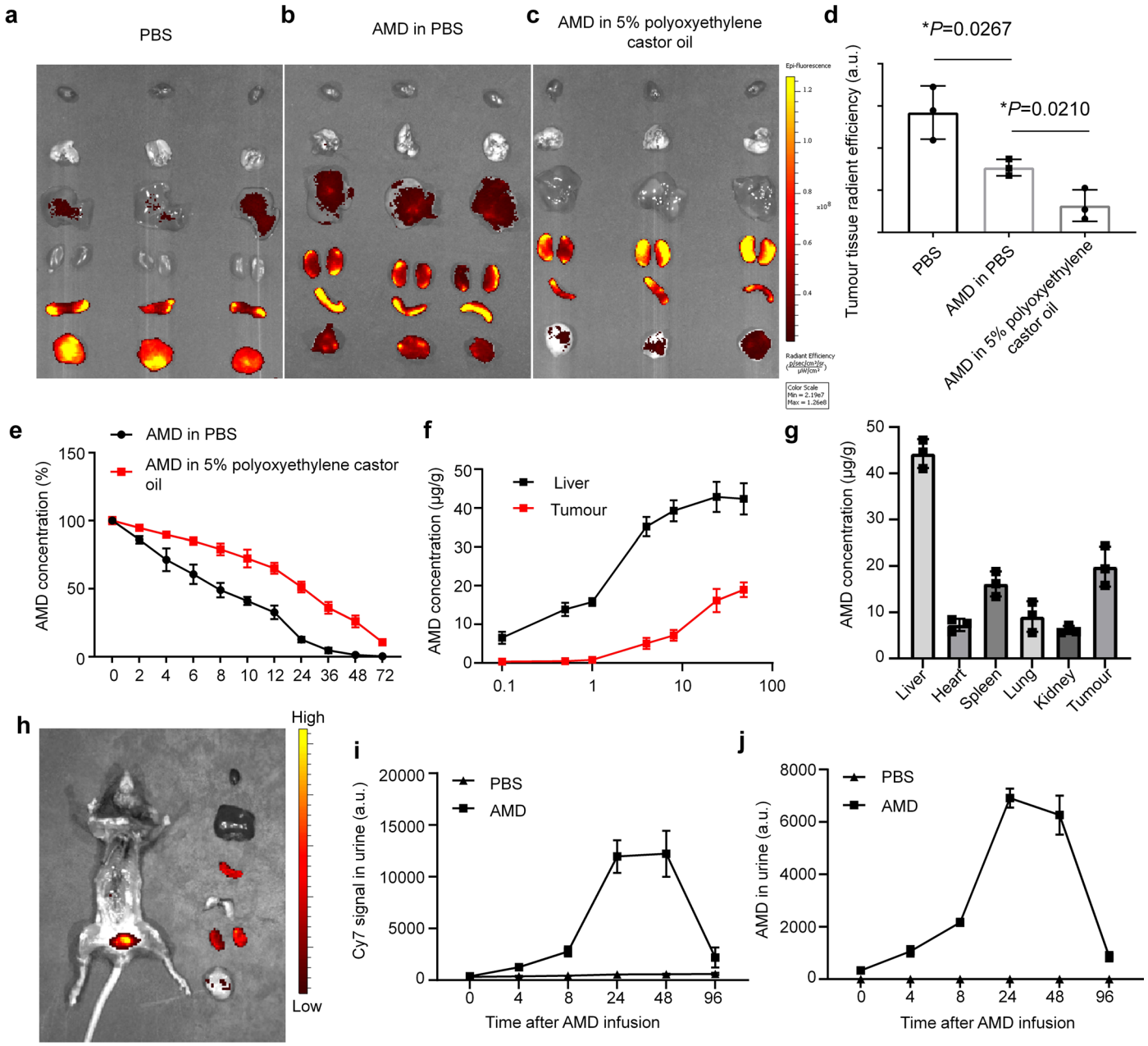

Extended Data Fig. 1 | AMD mediates the *in vivo* disassembly of SiTE. SiTE was labelled with Cy7 dye (Cy7 was labelled on CD3 Fab) and was i.v. injected to tumour-bearing mice at 0h. Then, PBS, AMD dispersed in PBS or AMD dispersed in 5% polyoxyethylene castor oil was injected at 18 h post-SiTE-Cy7 injection. 6 h later, mice were euthanized and the Cy7 signal in different organs and tumour was measured using IVIS (**a**-**c**). **d**, quantification of the fluorescence in tumour tissues in **a**-**c**. Data was shown as mean ± SD (n = 3), statistical differences were analysed using two-tailed unpaired Student's *t*-test. **e**, Half-life of AMD in mouse blood when the AMD is dispersed in PBS or in 5% polyoxyethylene castor oil. When the AMD is dispersed in PBS, the half-life is about 9 hours, which is increased to 24 h when it is dispersed in 5% polyoxyethylene castor oil. **f**, AMD concentrations in the liver and tumour over time were investigated. **g**, the distribution of AMD in mouse tumours and major organs after 24h of AMD infusion. **h**, In order to investigate the clearance of the disassembled SiTE and the AMD, we performed another animal experiment. SiTE-Cy7 was i.v. infused into tumour bearing mice at 0 h. 4 h later, AMD was infused. After 24 h, mice were euthanized and the Cy7 signal distribution in major organs and mouse whole body was observed. Cy7 signal was detected in the spleen, kidneys and bladder. This demonstrates the potential clearance from the kidneys and urine. We then performed a kinetics study to investigate the Cy7 signal (**i**) and AMD level in the urine (**j**).

https://doi.org/10.1038/s41551-023-01147-6

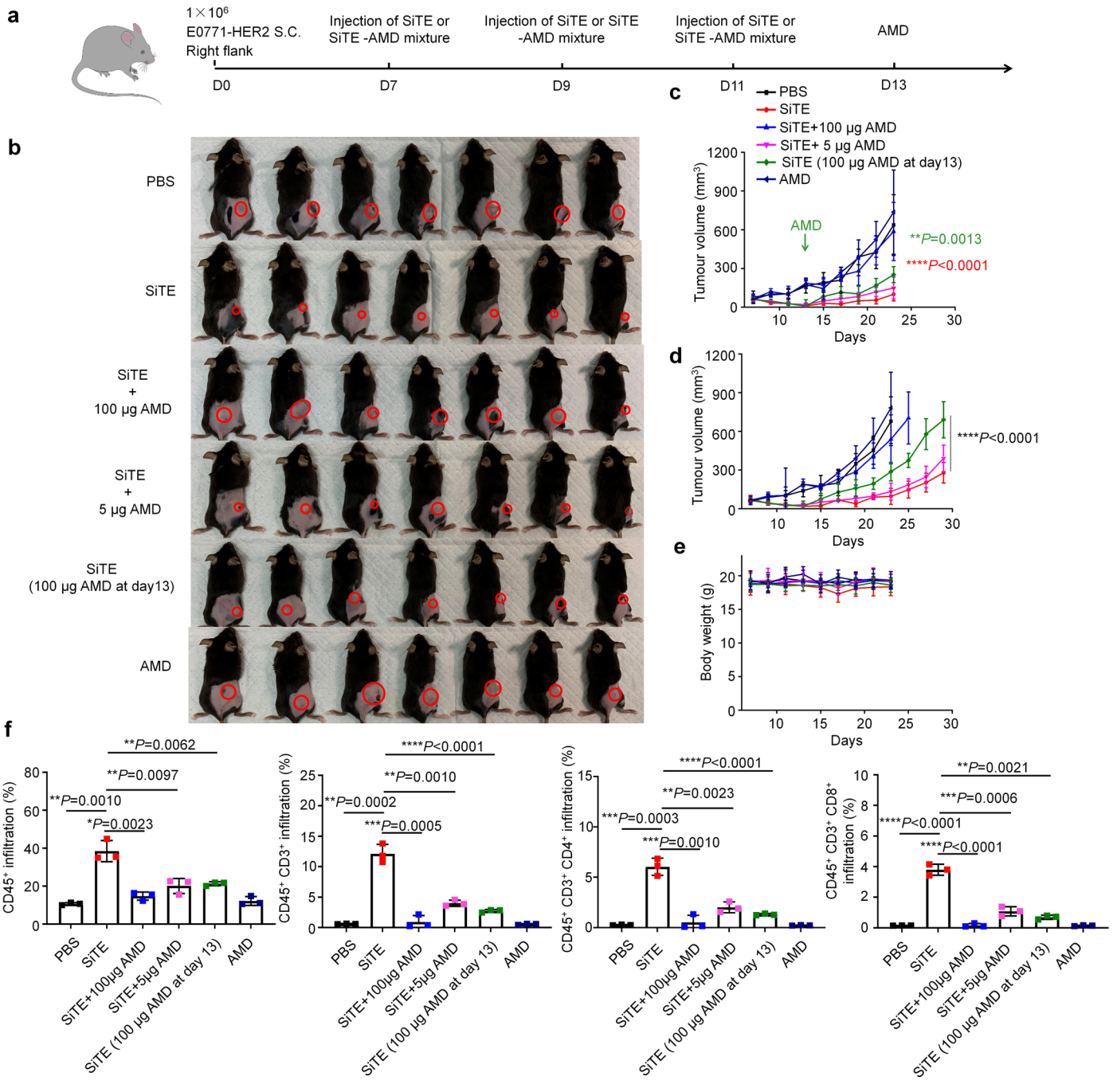

Extended Data Fig. 2 | AMD controls SiTE activity *in vivo*. **a**, 10^6 E0771-HER2 cells were s.c. injected into the right flank of C57/BL6 mice. When tumour sizes reached 50 mm^3 (Day 7), mice were given an i.v. injection of 100 μL of their respective treatments—PBS, SiTE, SiTE + 100 μg AMD, SiTE + 5 μg AMD, or 100 μg AMD (in 5% polyoxyethylene castor oil). One group received SiTE on day 7 followed by 100 μg AMD at day 13. All mice were euthanized at day 23. **b**, Images of mice from all treatment groups on day 23. **c,** tumour growth curves for different groups. Tumour tissue was isolated on day 23 and observed for immune cell infiltration. **d**, repeat of the tumour growth inhibition experiment. **e**, mouse body weight change during the tumour inhibition experiment. **f**, Percentages of $CD45^+$, $CD45^+CD3^+$, $CD45^+CD3^+CD4^+/CD8^+$ cells in the tumour tissues. **g**, Immunofluorescence images of the tumour tissues in different groups with cell nuclei labeled with DAPI (blue) and T cells labeled with anti-CD3 antibody (green). Scale bar: 100 μm. The statistical significance of tumour volume in **c** and **e** was analysed by two-tailed unpaired Student's *t*-test. $^{**}P = 0.0013$ $^{****}P<0.0001$. The statistical significance displayed in **f** was analysed by two-tailed unpaired Student's *t*-test.

https://doi.org/10.1038/s41551-023-01147-6

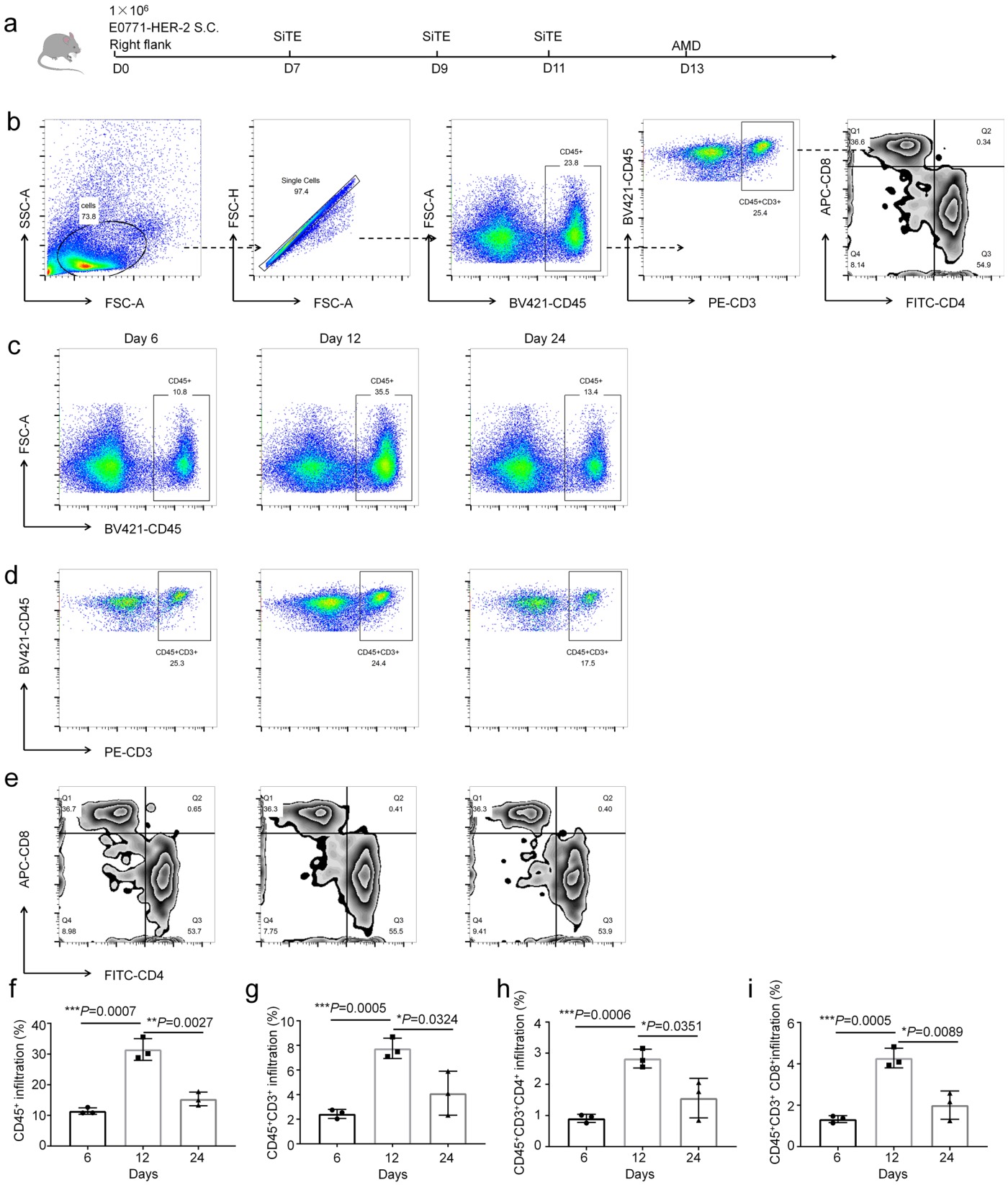

Extended Data Fig. 3 | T-cell infiltration levels in the tumour tissues before and after SiTE or AMD treatment. The mice were s.c injected with 10^6 E0771-HER2 cells at day 0, SiTE was injected at day 7, 9, and day 11 and AMD was injected at day 13 **a**, The tumour tissues at day 6, day 12 and day 14 were collected, digested, and filtered, and the immune cell infiltration in the tumour tissue was analysed using flow (flow gating strategy is shown in **b**). **c**, **d**, and **e** are flow dot plots of $CD45^+$, $CD45^+CD3^+$, $CD45^+CD3^+CD4^+$ or $CD45^+CD3^+CD8^+$ cells, respectively. **f-i** are quantifications of **c-e**, respectively. The statistical significance of tumour volume in **f-i** was analysed by two-tailed unpaired Student's *t*-test. **f**, $^{***}P = 0.0007$, $^{**}P = 0.0027$. **g**, $^{***}P = 0.0005$, $^{*}P = 0.0324$. **h**, $^{***}P = 0.0006$, $^{*}P = 0.0351$. **i**, $^{***}P = 0.0005$, $^{*}P = 0.0089$.

https://doi.org/10.1038/s41551-023-01147-6

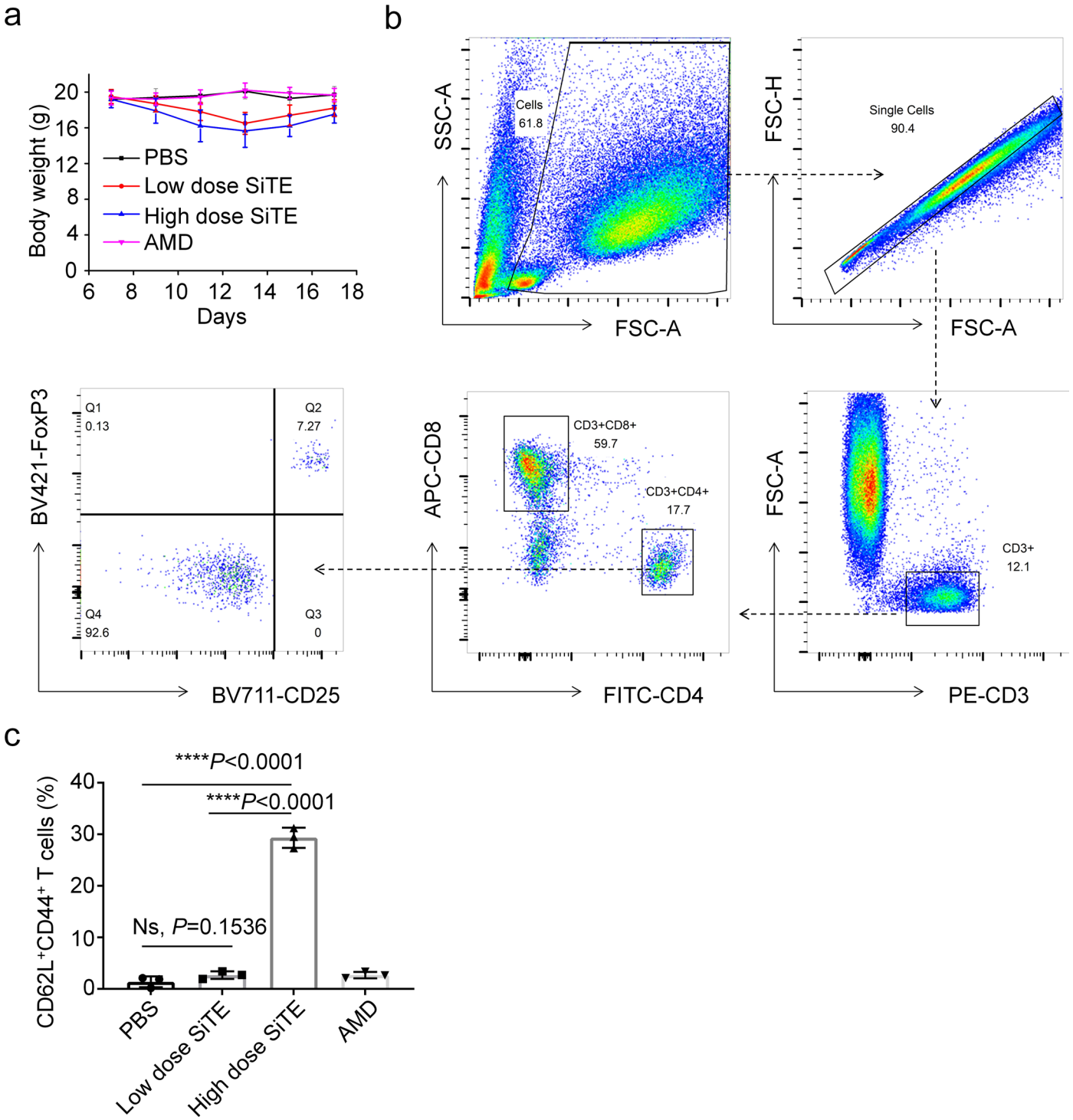

Extended Data Fig. 4 | High dose of SiTE elicited antigen-specific immune response to tumours. C57BL/6 mice with liver expression of HER2 were injected with PBS, SiTE low dose, SiTE high dose, or AMD at days 7, 9 and 11. AMD was administered to SiTE-treated groups once severe toxicity was observed. Mice were euthanized at day 17, and the tumour tissues were collected and analysed by flow cytometry. **a,** mouse weight during the treatment. **b,** flow gating strategy. **c,** $CD44^+CD62L^+$ central memory cells in the tumour tissue.

https://doi.org/10.1038/s41551-023-01147-6

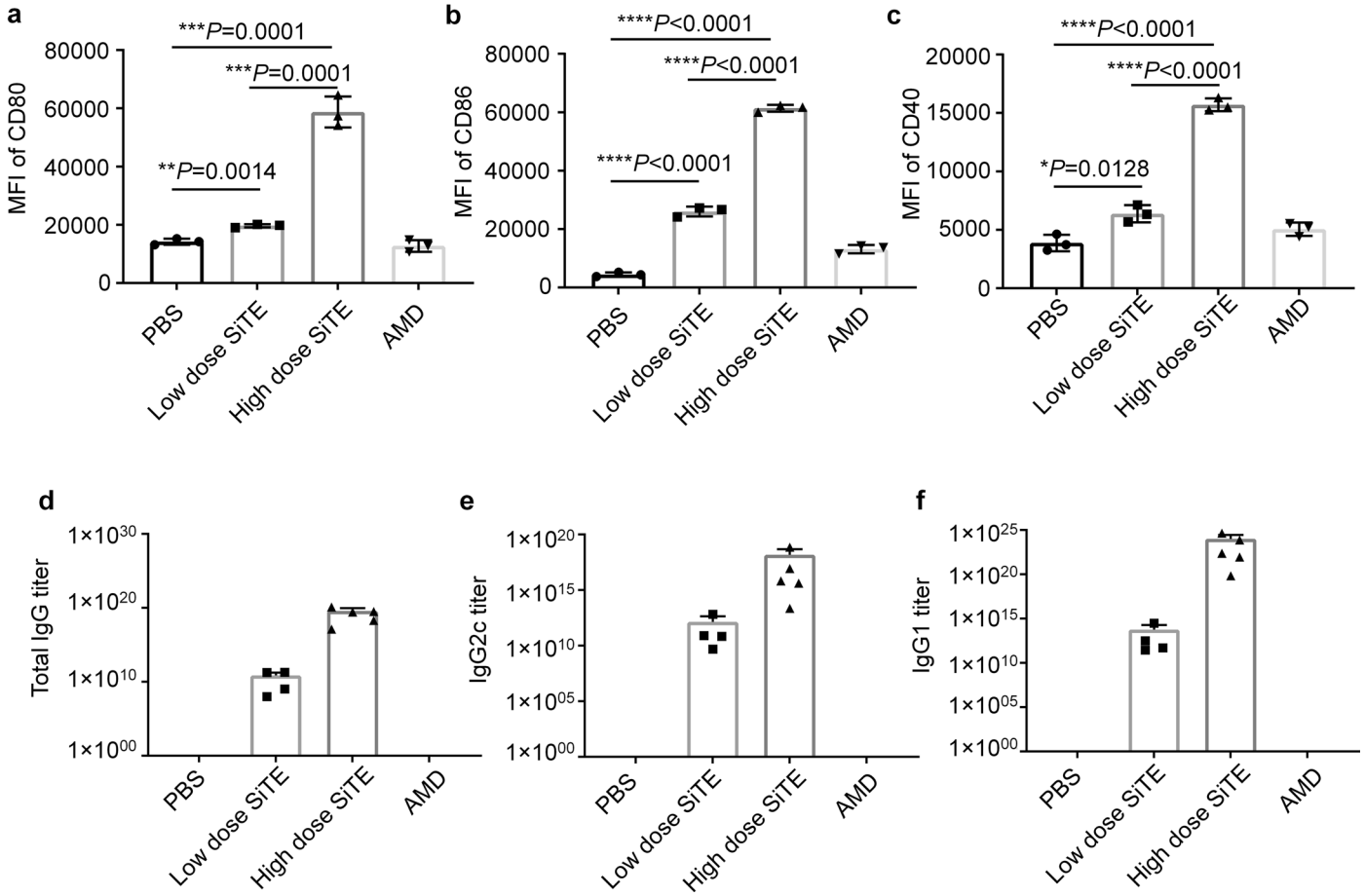

Extended Data Fig. 5 | High doses of SiTE enhance DC maturation and antibody production *in vivo*. **a-c**, E0771-HER2 cells were s.c. injected to mice at day 0. E0771-HER2 tumour-bearing mice were treated with low doses (1 mg/kg) or high doses (5 mg/kg) of SiTE at days 7, 9, and 11. AMD was infused at day 13. Mice were euthanized at day 13 and the dendritic cell maturation levels in the tumour draining lymph nodes were evaluated. PBS or AMD-only were used as two control groups. **d-f**, In order to investigate the humoral immune response induced by SiTE, E0771-HER2 tumour-bearing mice were treated with low doses (1 mg/kg) or high doses (5 mg/kg) of SiTE at days 7, 9, and 11. AMD was infused at day 13. At day 27, the HER2-specific total IgG, IgG2c, and IgG1 levels in mouse blood were determined. *P* values were indicated in **a-c**, analysed by two-tailed unpaired Student's *t*-test. n = 3.

https://doi.org/10.1038/s41551-023-01147-6

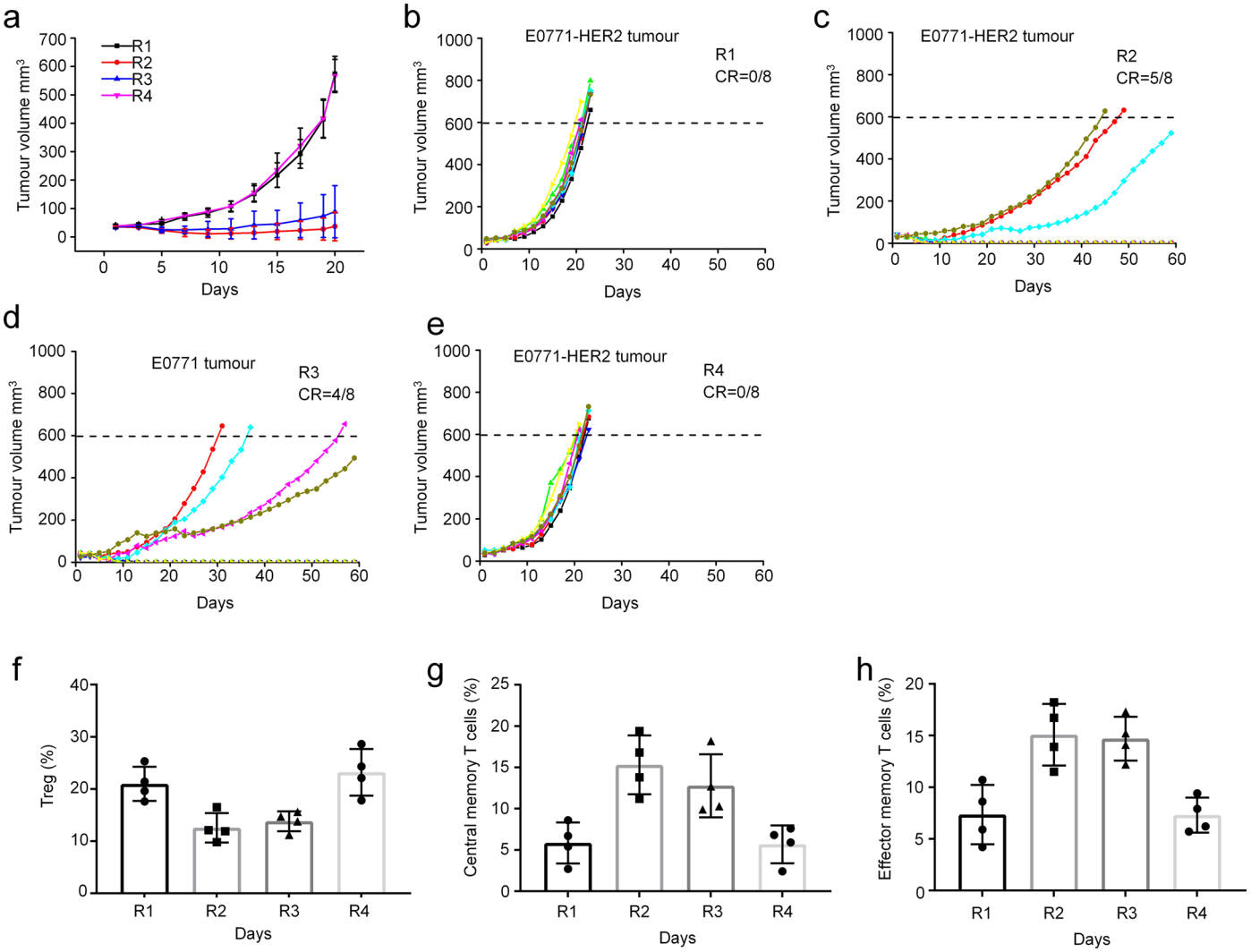

Extended Data Fig. 6 | Tumour-cell-rechallenging experiment. Tumour-free mice from the high dose group were rechallenged with E0771-HER2 or E0771 cells and compared to mice pre-treated with either PBS or AMD challenged with E0771-HER2 as controls. Group R1: Healthy mice were treated with PBS at days −43, −41, and −39. The mice were i.v. injected with E0771-HER2 cells at day 0; Group R2: E0771-HER2 tumour-bearing mice were treated with a high dose of SiTE at days −43, −41, and −39, AMD was i.v. injected at day −37. The tumour-free mice were rechallenged with E0771-HER2 cells at day 0; Group R3, E0771-HER2 tumour-bearing mice were pre-treated with high dose of SiTE at days −43, −41, and −39. AMD was i.v. injected at day −37. The mice were rechallenged with E0771-HER2 cells at day 0. Group R4, healthy mice were treated with AMD at day −37 and the mice were i.v. injectied with E0771-HER2 cells at day 0. **b**-**e** are individual E0771-HER2 or E0771 tumour size curves in the different treatment groups. CR, complete regression (n = 8). The mice were euthanized, and the immune cell infiltration in the tumour tissue was analysed using flow. **f**-**h,** Treg percentages, $CD44^+CD62L^+$ central memory T cell percentages, and $CD44^+CD62L^-$ effector memory T cells in different treatment groups, respectively. Data were shown as mean ± SD, n = 4.

https://doi.org/10.1038/s41551-023-01147-6

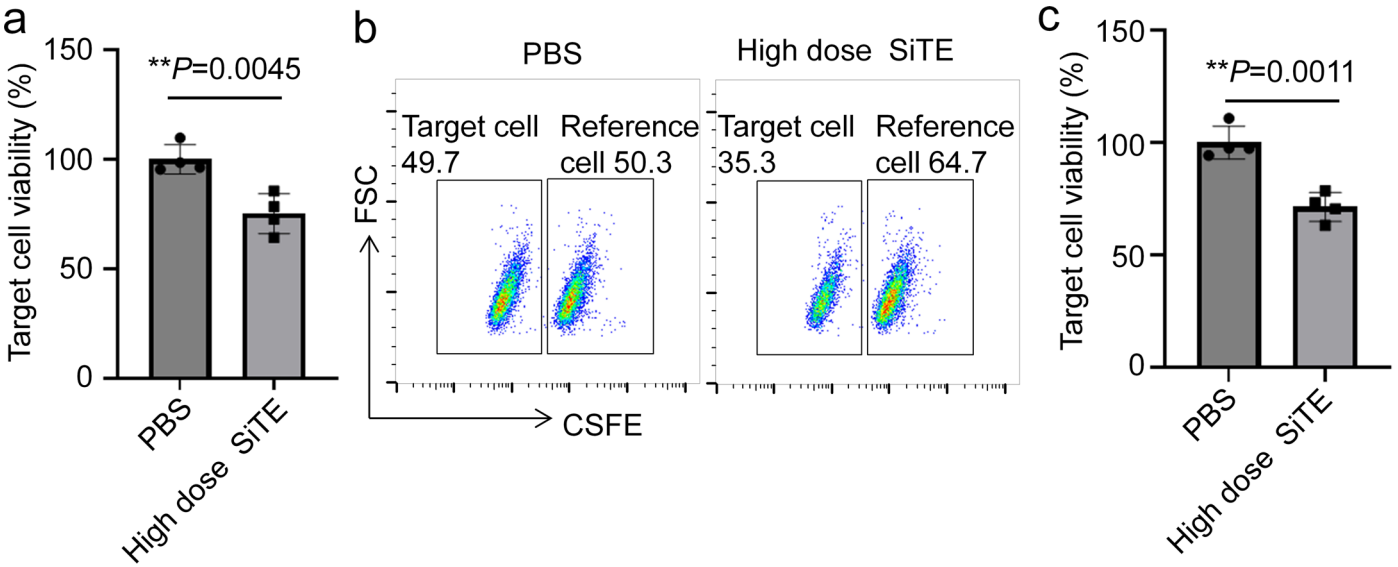

Extended Data Fig. 7 | High doses of SiTE generate tumour-specific T-cell immune responses. E0771-HER2 tumour-bearing mice were treated with high doses of SiTE. 7 days-post the last dose, T cells were collected from the mice and were co-cultured with E0771-HER2 cells (express luciferase) for 24h. E0771-HER2 cell viability was determined (**a**). **b** and **c**, E0771-HER2 target cells (labelled with low level of CSFE) and reference cells (B16 cell line, labelled with high level of CSFE) were i.v. infused into the high dose SiTE-treated mice mentioned above. 24 later, target cell killing was determined using flow cytometry (**b**). **c**, quantification of **b**. Data in **a** and **c** are shown as mean ± SD, n = 4. *P* values in **a** and **c** was determined using two-tailed unpaired student's *t*-test.

https://doi.org/10.1038/s41551-023-01147-6

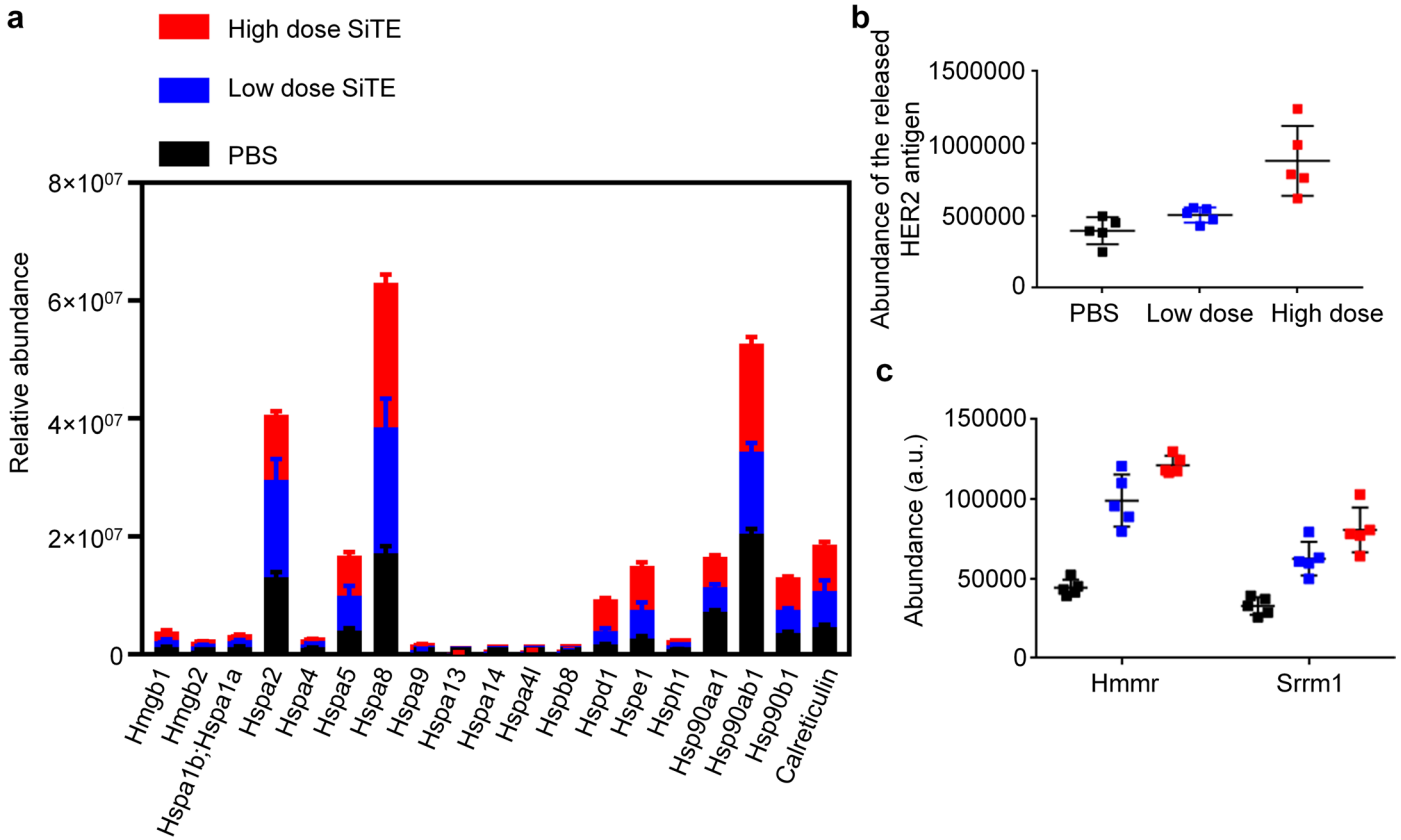

Extended Data Fig. 8 | Proteomics shows that a high dose of SiTE treatment induces damage-associated molecular patterns (DAMPs) and tumour-antigen release. E0771-HER2 cells were incubated with mouse T cells in serum-free medium and were treated with a low dose (5 ng/mL) or a high dose (20 ng/mL) of SiTE. After 24h, the supernatant was collected and the proteins in the medium were analysed. **a**, relative abundance of various DAMPs released to cell culture medium in the high dose SiTE, low dose SiTE or PBS-treated group. **b**, and **c**, tumour antigen HER2 and tumour neoantigen hmmr and srrm1 abundance in the cell culture medium in different groups.

https://doi.org/10.1038/s41551-023-01147-6

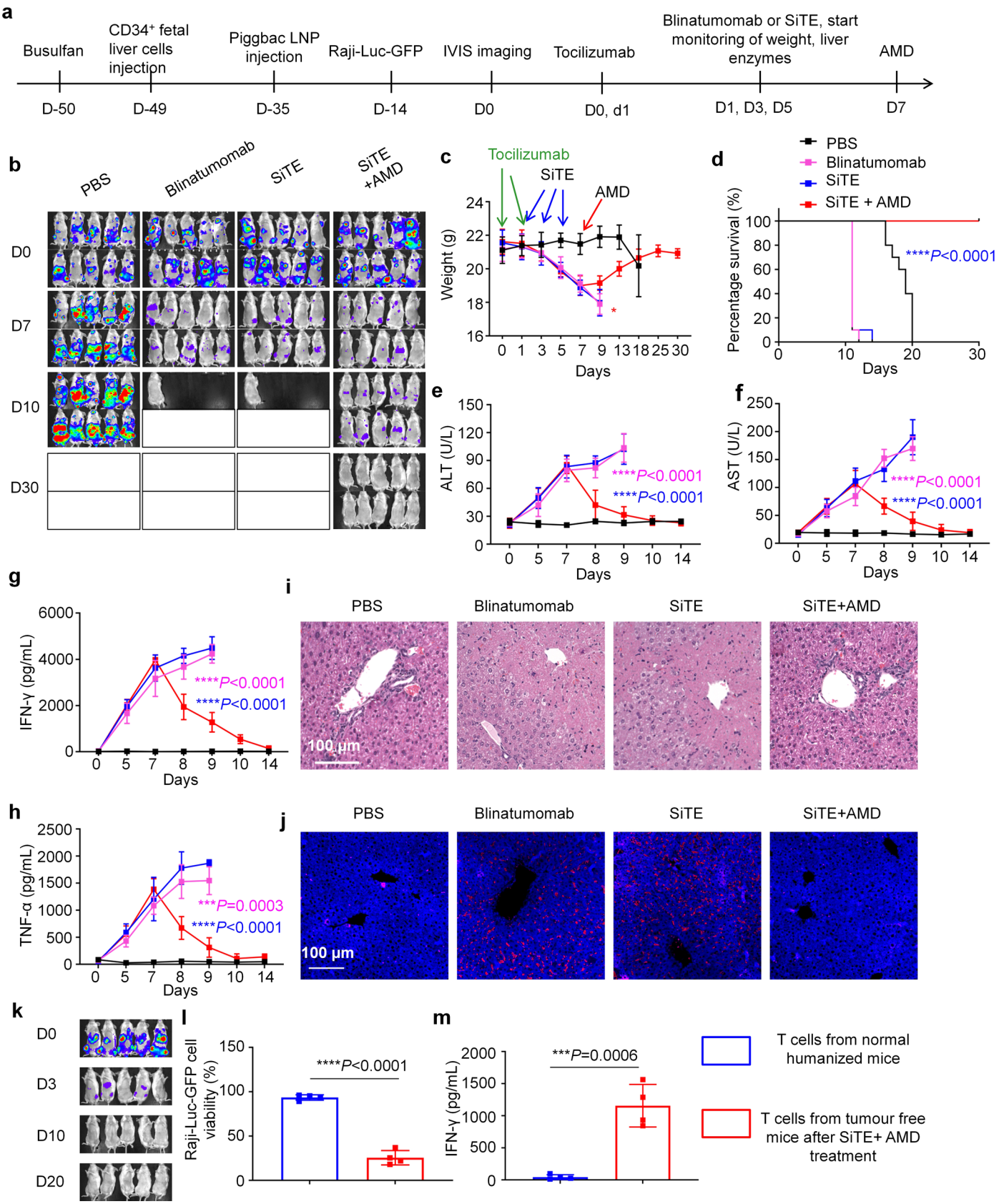

Extended Data Fig. 9 | See next page for caption.

https://doi.org/10.1038/s41551-023-01147-6

Extended Data Fig. 9 | AMD reduces the on-target off-tumour toxicity of SiTE *in vivo*. **a**, A humanized immune system mouse model was constructed by treating the mice with an i.p. injection of Busulfan at day −50 followed by an i.v. injection of 10^5 human $CD34^+$ foetal liver cells at day −49. Human CD19 antigen was expressed in the livers of the mice using a piggyBac transposon system delivered via lipid nanoparticles (LNPs) encapsulating two plasmids, pCMV-hyPBase and pPB CMV-hCD19:T2A:EGFP, at day −35. At day −14, 10^6 Raji-Luc-GFP tumour cells were i.v. injected. Before using Blinatumomab or SiTE for cancer treatment, Tocilizumab (10 mg/kg) was administered to mice to prevent CRS-related symptoms. PBS, Blinatumomab in vivo bio-similar antibody (5 mg/kg), or SiTE (5 mg/kg) were i.v. injected every two days for three total doses. When an approximate 15% decrease in body weight (indicative of toxicity) was observed on day 7, half of the mice that had received SiTE were given an i.v. injection of AMD (in 5% polyoxyethylene castor oil). Throughout the study, mice were euthanized when body weight decreased more than 20%. IVIS was used to monitor tumour burden in vivo. **b,** IVIS images of the mice at days 0, 7, 10, and 30. **c**, and **d**, Mouse body weight and survival curves, respectively. n = 10 mice. The red stars in **b** and **c** indicate that mice were euthanized. **e**-**h**, Measurements for markers of toxicity and inflammation including AST, ALT, TNF-α, IFN-γ levels in mouse blood at different time points. n = 10 mice. **i**, In order to evaluate liver toxicity induced by various treatments, an additional animal experiment was performed and mouse livers were harvested at day 9. H&E staining was conducted to detect liver damage in different groups. Scale bar: 100 μm. **j**, Immunofluorescence imaging of $CD3^+$ T cells in liver tissue. Blue: DAPI; Red, $CD3^+$ T cells. **k**, tumour-free mice from the SiTE+AMD group were rechallenged with 10^6 Raji-Luc-GFP cells and the tumour burden post Raji-Luc-GFP cell rechallenging was monitored with IVIS. **l**-**m**, T cells in the tumour-free mice from the SiTE+AMD group were sorted and were co-cultured with Raji-Luc-GFP cells for 24 h and tumour cell viability was determined using a luciferase assay kit (**l**). T cells from normal humanized mice co-cultured with Raji-Luc-GFP cells were used as a control group. **m**, IFN-γ concentrations in the cell culture medium were determined using an ELISA kit. The data in **e**-**h** were plotted as mean ± s.d. (n = 10) from three independent experiments. *P* values indicated in **e**-**h** were analysed by two-tailed unpaired Student's *t*-test. Pink, Blinatumomab vs SiTE + AMD at day 9; blue, SiTE vs SiTE + AMD at day 9; $^{***}P = 0.0003$, $^{****}P<0.0001$. *P* value in **d** was determined using Log-rank (Mantel-Cox) test, $^{****}P<0.0001$. *P* values in **l** and **m** were determined by two-tailed unpaired Student's *t*-test, $^{****}P<0.0001$, $^{***}P = 0.0006$.

https://doi.org/10.1038/s41551-023-01147-6

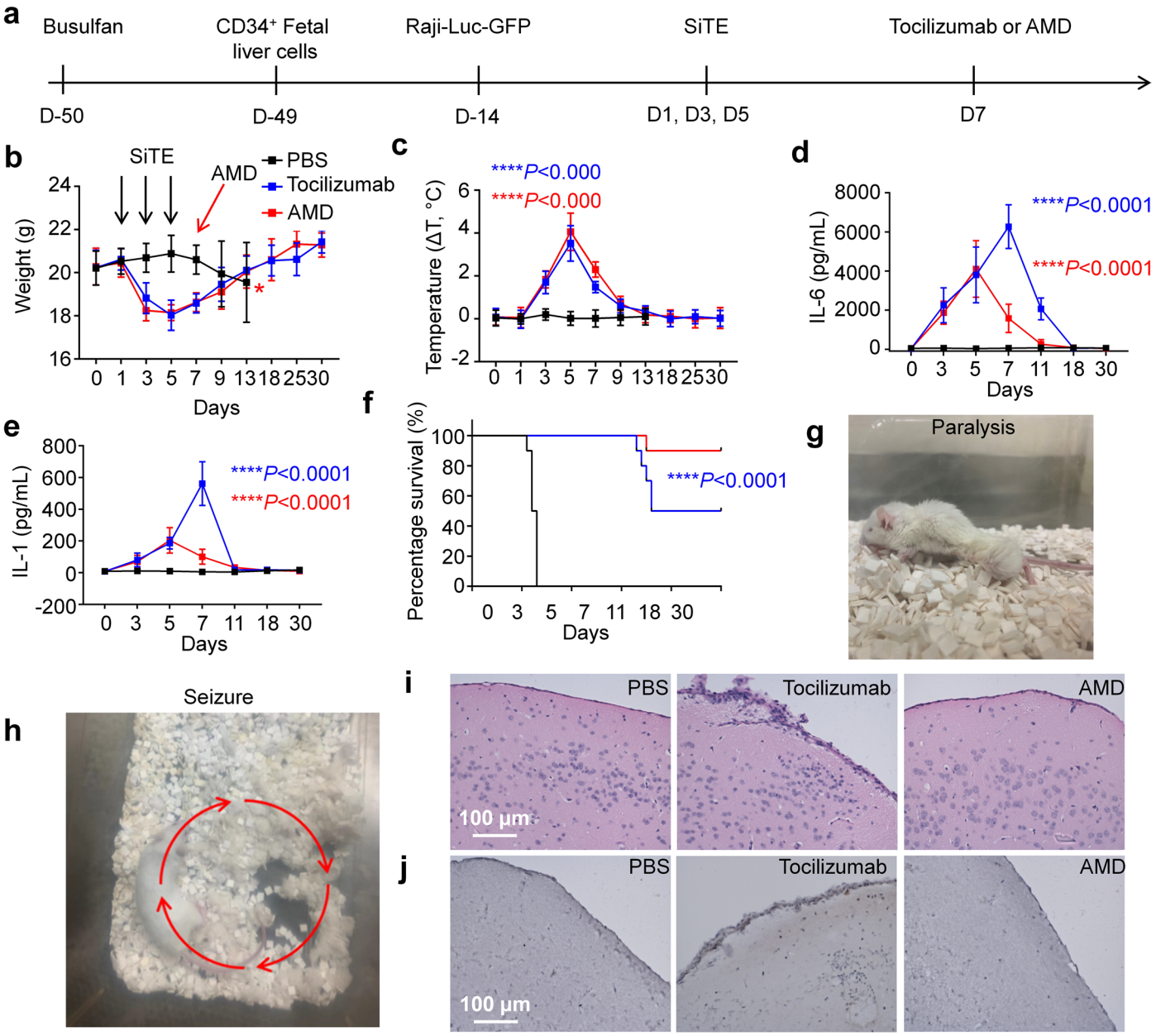

Extended Data Fig. 10 | AMD reduces SiTE-induced neurotoxicity *in vivo*. **a**, NSG-SGM3 mice were treated with Busulfan at day −50 to remove mouse bone marrow. At day −49, 10^5 human CD34$^+$ foetal liver cells were i.v. injected to allow the mouse develop a human immune system. 10^6 Raji-Luc-GFP tumour cells were i.v. injected at day −14. At days 1, 3, and 5, PBS or SiTE was i.v. injected (in the PBS group, only PBS was injected into tumour-bearing mice). When an approximate 15% decrease in body weight (indicative of toxicity) was observed on day 7, half of the mice that had received SiTE were given an i.v. injection of AMD (10 mg/kg) and half of them were given Tocilizumab (10 mg/kg) for CRS treatment. **b**, **c**, **d**, and **e**, Mouse body weight, temperature, IL-6 levels, and mouse survival curves, respectively. n = 10 mice. The red stars in **b** indicate that mice were euthanized. **f**, Measurements of IL-1 in mouse blood at different time points. n = 10 mice. At around day 33 post-SiTE injection, humanized NSG-SGM3 mice that received either PBS or Tocilizumab treatment developed paralysis (**g**) or experienced a seizure as indicated by movement along the red arrows (**h**), which are signs of lethal neurological syndrome. However, mice treated with AMD did not develop paralysis and were not observed to experience seizures indicative of lethal neurological syndrome. Brain H&E staining (**i**) and human CD68 immunohistochemistry (**j**) images of mice at day 35. The data in **b**-**f** were plotted as mean ± s.d. (n = 10) from three independent experiments. *P* value in **f** was determined using Log-rank (Mantel-Cox) test, $^{****}P < 0.0001$.

nature portfolio

Corresponding author(s): Michael Mitchell

Last updated by author(s): Oct 20, 2023

Reporting Summary

Nature Portfolio wishes to improve the reproducibility of the work that we publish. This form provides structure for consistency and transparency in reporting. For further information on Nature Portfolio policies, see our Editorial Policies and the Editorial Policy Checklist.

Statistics

For all statistical analyses, confirm that the following items are present in the figure legend, table legend, main text, or Methods section.

n/a	Confirmed	
☐	☒	The exact sample size (*n*) for each experimental group/condition, given as a discrete number and unit of measurement
☐	☒	A statement on whether measurements were taken from distinct samples or whether the same sample was measured repeatedly
☐	☒	The statistical test(s) used AND whether they are one- or two-sided *Only common tests should be described solely by name; describe more complex techniques in the Methods section.*
☐	☒	A description of all covariates tested
☐	☒	A description of any assumptions or corrections, such as tests of normality and adjustment for multiple comparisons
☐	☒	A full description of the statistical parameters including central tendency (e.g. means) or other basic estimates (e.g. regression coefficient) AND variation (e.g. standard deviation) or associated estimates of uncertainty (e.g. confidence intervals)
☐	☒	For null hypothesis testing, the test statistic (e.g. *F*, *t*, *r*) with confidence intervals, effect sizes, degrees of freedom and *P* value noted *Give P values as exact values whenever suitable.*
☒	☐	For Bayesian analysis, information on the choice of priors and Markov chain Monte Carlo settings
☒	☐	For hierarchical and complex designs, identification of the appropriate level for tests and full reporting of outcomes
☒	☐	Estimates of effect sizes (e.g. Cohen's *d*, Pearson's *r*), indicating how they were calculated

Our web collection on statistics for biologists contains articles on many of the points above.

Software and code

Policy information about availability of computer code

Data collection	ZEN2010, MestReNova 9.0, Flowjo V10, IVIS specturm 4.0,
Data analysis	Statistical analyses were performed on Graphpad Prism 7.0. Flow-cytometry data were analysed using the FlowJo software package (Flowjo V10).

For manuscripts utilizing custom algorithms or software that are central to the research but not yet described in published literature, software must be made available to editors and reviewers. We strongly encourage code deposition in a community repository (e.g. GitHub). See the Nature Portfolio guidelines for submitting code & software for further information.

Data

Policy information about availability of data

All manuscripts must include a data availability statement. This statement should provide the following information, where applicable:

- Accession codes, unique identifiers, or web links for publicly available datasets
- A description of any restrictions on data availability
- For clinical datasets or third party data, please ensure that the statement adheres to our policy

The data supporting the results in this study are available within the paper and its Supplementary Information. Source data for the figures are provided with this paper. The raw and analysed datasets generated during the study are available for research purposes from the corresponding authors on reasonable request.

Field-specific reporting

Please select the one below that is the best fit for your research. If you are not sure, read the appropriate sections before making your selection.

☒ Life sciences ☐ Behavioural & social sciences ☐ Ecological, evolutionary & environmental sciences

For a reference copy of the document with all sections, see nature.com/documents/nr-reporting-summary-flat.pdf

Life sciences study design

All studies must disclose on these points even when the disclosure is negative.

Sample size	No effect size was predetermined, but the sample sizes employed in this study are consistent with previously published works (Li A. W. et al. Nat. Mater. 17, 528–534 (2018); Kuai R. et al. Nat. Mater. 16, 489–496 (2017)). For example, the in vitro studies were repeated at least three times independently, and in vivo experiments with 7–10 mice per group were performed.
Data exclusions	No animals and/or data were excluded.
Replication	All experiments were repeated at least three times, and the experimental findings were reproducible.
Randomization	The dosing groups were filled by randomly selecting from the same pool of animals for the in vivo experiments. Groups in all the in vitro and in vivo experiments were selected randomly.
Blinding	All the investigators were blinded to group allocation during data collection and analysis.

Reporting for specific materials, systems and methods

We require information from authors about some types of materials, experimental systems and methods used in many studies. Here, indicate whether each material, system or method listed is relevant to your study. If you are not sure if a list item applies to your research, read the appropriate section before selecting a response.

Materials & experimental systems

n/a	Involved in the study
☐	☒ Antibodies
☐	☒ Eukaryotic cell lines
☒	☐ Palaeontology and archaeology
☐	☒ Animals and other organisms
☒	☐ Human research participants
☒	☐ Clinical data
☒	☐ Dual use research of concern

Methods

n/a	Involved in the study
☒	☐ ChIP-seq
☐	☒ Flow cytometry
☒	☐ MRI-based neuroimaging

Antibodies

Antibodies used	Anti-human HER2 (Catalog: BE0277, clone: 7.16.4), anti-mouse CD3 (Catalog: BE001-1FAB, clone: 145-2C11 f(ab')2 Fragments) and anti-human CD3 (Catalog: BE0231, clone: UCHT1 (Leu-4) (T3)) antibodies were purchased from BioXcell. Flow antibodies anti-mouseCD45-Brilliant Violet 421 (Catalog: 103133, clone: 30-F11, 1:100 dilution), anti-mouseCD3-PE (Catalog: 100206, clone: 17A2,1:100 dilution), anti-mouseCD4-Alexa Fluor® 488 (Catalog: 100423, clone: GK1.5,1:100 dilution), anti-mouseCD8-APC (Catalog: 100712, clone: 53-6.7, 1:100 dilution), anti-mouseFoxP3-Brilliant Violet 421 (Catalog: 126419, clone: MF-14, 1:100 dilution), anti-mouseCD25-Brilliant Violet 711 (Catalog: 102049, clone: PC61, 1:100 dilution), anti-mouseCD44-Brilliant Violet 421 (Catalog: 103039, clone: IM7, 1:100 dilution), anti-mouseCD62L-Brilliant Violet 711 (Catalog: 104445, clone: MEL-14, 1:100 dilution) were purchased from Biolegend.
Validation	All antibodies were verified by the supplier and each lot has been quality tested. All the antibodies used are from commercial sources and have been validated by the vendors. Validation data are available on the manufacturer's website. 1. Anti-human HER2 antibody has been validated to be used for in vivo HER2 targeting applications and mentioned species reactivity with human. (https://bxcell.com/product/invivomab-anti-humanrat-her2-neu/, ref: Kodumudi K N, et al.. Frontiers in immunology, 2019, 10: 1939.) 2. Anti-mouse CD3 antibody has been validated to be used for in vivo CD3 targeting applications mentioned species reactivity with mouse. (https://bxcell.com/product/m-cd3e-fab2-fragments/, ref: Sarikonda G, et al. Journal of Autoimmunity, 2015, 59: 61-66.) 3. Anti-human CD3 antibody has been validated to be used for in vivo CD3 targeting applications and mentioned species reactivity with human. (https://bxcell.com/product/h-cd3-2/, ref: Wunderlich M, et al. Blood, 2014, 123(24): e134-e144.) 4. Anti-mouseCD45-Brilliant Violet 421 antibody has been validated to be used flow cytometric analysis and mentioned species reactivity with mouse. (https://www.biolegend.com/en-us/products/brilliant-violet-421-anti-mouse-cd45-antibody-7253, ref: Radtke A J, et al. Nature Protocols, 2022, 17(2): 378-401.) 5. Anti-mouseCD3-PE antibody has been validated to be used flow cytometric analysis and mentioned species reactivity with mouse.

(https://www.biolegend.com/en-us/products/pe-anti-mouse-cd3-antibody-47, ref: Radtke A J, et al. Nature Protocols, 2022, 17(2): 378-401.)
6. Anti-mouseCD4-Alexa Fluor® 488 antibody has been validated to be used flow cytometric analysis and mentioned species reactivity with mouse. (https://www.biolegend.com/en-us/products/alexa-fluor-488-anti-mouse-cd4-antibody-2695, ref: Felix N J, et al. Nature immunology, 2007, 8(4): 388-397.)
7. Anti-mouseCD8-APC antibody has been validated to be used flow cytometric analysis and mentioned species reactivity with mouse. (https://www.biolegend.com/en-us/products/apc-anti-mouse-cd8a-antibody-150, ref: Rasmussen J W, et al. Infection and immunity, 2006, 74(12): 6590-6598.)
8. Anti-mouseFoxP3-Brilliant Violet 421 antibody has been validated to be used flow cytometric analysis and mentioned species reactivity with mouse. (https://www.biolegend.com/en-us/products/brilliant-violet-421-anti-mouse-foxp3-antibody-12143, ref: Nakashima H, et al. The Journal of Immunology, 2010, 184(9): 4637-4645.)
9. Anti-mouseCD25-Brilliant Violet 711 antibody has been validated to be used flow cytometric analysis and mentioned species reactivity with mouse. (https://www.biolegend.com/en-us/products/brilliant-violet-711-anti-mouse-cd25-antibody-10292, ref: Liu F, et al. Archives of toxicology, 2011, 85: 1383-1394.)
10. Anti-mouseCD44-Brilliant Violet 421 antibody has been validated to be used flow cytometric analysis and mentioned species reactivity with mouse. (https://www.biolegend.com/en-us/products/brilliant-violet-421-anti-mouse-human-cd44-antibody-7225, ref: Wang X Y, et al. Blood, 2008, 111(4): 2436-2443.)
11. Anti-mouseCD62L-Brilliant Violet 711 antibody has been validated to be used flow cytometric analysis and mentioned species reactivity with mouse. (https://www.biolegend.com/en-us/products/brilliant-violet-711-anti-mouse-cd62l-antibody-10317, ref: Si Y, Tian Q, et al. Science advances, 2020, 6(32): eaba0995.)

Eukaryotic cell lines

Policy information about cell lines

Cell line source(s)	E0771 and E0771-HER2 cells were requested from Betty Y. S. Kim. Raji-Luc-GFP cells were requested from Alan Epstein.
Authentication	A short-tandem-repeat DNA-profiling method was used to authenticate the cell lines, and the results were compared with a reference database.
Mycoplasma contamination	All cell lines were tested for mycoplasma contamination. No mycoplasma contamination was found.
Commonly misidentified lines (See ICLAC register)	The E0771, E0771-HER2, Raji and Raji-luc-gfp cell lines are not listed in the database.

Animals and other organisms

Policy information about studies involving animals; ARRIVE guidelines recommended for reporting animal research

Laboratory animals	C57BL/6 and NSG-SGM3 mice (female, 6–8 weeks, around 20 g) were ordered from The Jackson laboratory and housed in a specific-pathogen-free animal facility at ambient temperature (22 ± 2 °C), air humidity 40%–70% and a 12-h-dark/12-h-light cycle.
Wild animals	The study did not involve wild animals.
Field-collected samples	The study did not involve samples collected from the field.
Ethics oversight	All animal experiment protocols were reviewed and approved by the institutional animal care and use committee of the University of Pennsylvania.

Note that full information on the approval of the study protocol must also be provided in the manuscript.

Flow Cytometry

Plots

Confirm that:

☒ The axis labels state the marker and fluorochrome used (e.g. CD4-FITC).

☒ The axis scales are clearly visible. Include numbers along axes only for bottom left plot of group (a 'group' is an analysis of identical markers).

☒ All plots are contour plots with outliers or pseudocolor plots.

☒ A numerical value for number of cells or percentage (with statistics) is provided.

Methodology

Sample preparation	For tumour samples, they were chemically disrupted and filtered through a 70-μM strainer. Then the suspensions were incubated with ammonium chloride buffer for erythocyte lysis, and washed with PBS. Single-cell suspensions were obtained and stained with antibodies according to the manufacturer's protocols, and then analysed by flow cytometry.
Instrument	BD LSR II
Software	FlowJo software package (Flowjo V10).

Cell population abundance	The absolute cells around 8,000–10,000 were analysed for fluorescent intensity in the defined gate.
Gating strategy	In general, cells were first gated on FSC/SSC. Singlet cells were gated using FSC-H and FSC-A. Dead cells were then excluded and further surface and intracellular antigen gating were performed on the live-cell population (Supplementary Figs. 16a, 20a and 23).

☒ Tick this box to confirm that a figure exemplifying the gating strategy is provided in the Supplementary Information.